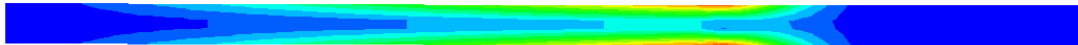


Fracture Analysis of Adhesive Joints using the Finite Element Method



Per Hansson

February 2002

Thesis for the Degree of Master of Science

Division of Solid Mechanics
Lund Institute of Technology

Division of Solid Mechanics

ISRN LUTFD2/TFHF--02/5093--SE (1-54)

**FRACTURE ANALYSIS OF ADHESIVE
JOINTS USING
THE FINITE ELEMENT METHOD**

Master's Dissertation by
Per Hansson

Supervisors
Solveig Melin, Div. of Solid Mechanics

Copyright © 2002 by Div. of Solid Mechanics,
Per Hansson

For information, address:
Division of Solid Mechanics, Lund University, Box 118, SE-221 00 Lund, Sweden.
Homepage: <http://www.solid.lth.se>

Preface

This master thesis is the final part of the Master in science program in Mechanical Engineering at Lund Institute of technology. The thesis work is assigned 20 credit points, which correspond to one semester.

The present work was carried out at the Division of Solid Mechanics at Lunds University under supervision of Solveig Melin.

First of all, I would like to thank my thesis adviser Solveig Melin for her invaluable advice and support during the project. Furthermore, I would like to thank Michael Andersson for his help and consultation concerning ABAQUS 5.8.

Lund, Sweden
February 2002

Per Hansson

Abstract

The behaviour of adhesive joints have been investigated. Two different adhesive/adherent systems consisting of toughened epoxy and steel, the Double Cantilever Beam (DCB) and the lap joint were investigated using the finite element method. In order to describe fracture of the adhesive a specially designed finite element, holding a cohesive zone, was introduced. Two different cohesive models were considered. The two models are different ways of describing the relation between the crack opening displacement and the stress. Such special crack elements were then implemented in the finite element models and placed along different predetermined crack paths. In order to find suitably crack paths a simple finite element analysis of the two different models were performed. Several different adhesive thicknesses were also investigated in order to determine the influence of adhesive thickness in the two adhesive/adherent systems and the displacements along the adhesive were investigated.

From the analysis of the DCB model, it was concluded that the adhesive thickness had small or no effect on the behaviour of the joint. A value of the critical load, at which the crack starts to grow, was determined and it appeared that the same critical load applied to the different crack paths. It was also concluded that the choice of plane stress or plane strain influenced the behaviour very little.

In the analysis of the lap joint divergence appeared and the simulations could not be completed and critical load could therefore not be determined. From the analysis it was concluded that an increasing adhesive thickness results in increasing separation of the adherents.

Contents

Preface.....	III
Abstract.....	V
Contents.....	VII
1. Introduction	1
2. Statement of the problem	3
3. Fracture modes	5
3.1 The strip yield model.....	5
3.2 Model A.....	6
3.3 Model B.....	8
3.4 Failure criterion.....	9
4. Finite element implementation.....	11
4.1 Crack element.....	12
4.1.1 Crack element description.....	12
4.1.2 Element formulation.....	13
5. Analysis of uncracked specimens	15
5.1 Stress distribution in the DCB-specimen	15
5.1.1 Stress analysis	15
5.1.2 Boundary conditions	15
5.1.3 Results	15
5.1.3.1 The von Mises equivalent stress.....	16
5.1.3.2 Normal stress in the 1-direction	17
5.1.3.3 Normal stress in the 2-direction	18
5.1.3.4 Shear stress distrubution.....	19
5.2 Stress distribution in the lap joint	
5.2.1 Stress analysis	21
5.2.2 Boundary conditions	21
5.2.3 Results	21
5.2.3.1 The von Mises equivalent stress.....	22
5.2.3.2 Normal stress in the 1-direction	23
5.2.3.3 Normal stress in the 2-direction	24
5.3 Crack path prediction	25

6. Fracture analysis of the DCB-specimen.....	27
6.1 Comparison between plane stress and plane strain elements.....	27
6.2 Influence of choice of stress-separation law	28
6.3 Crack path along symmetry line, variable thickness of the adhesive.....	31
6.4 Crack path along the interface, variable thickness of the adhesive.....	31
6.5 Influence of different shape parameters in model B	31
6.6 Verification of the finite element model	32
7. Fracture analysis of the lap joint	35
7.1 Crack path along the middle of the adhesive layer	35
7.2 Crack path along the interface.....	36
7.3 Displacements in the adhesive	37
8. Summary and discussion.....	41
9. Conclusion.....	43
10. References	45

1. Introduction

Techniques for joining two materials by a third phase have been used for a long time in a variety of industrial and technological applications. These techniques include traditional adhesive bonding, brazing, soldering, welding, riveting etc. The latest development in vehicle design, especially for cars and airplanes, strives toward products with low weight and high strength. This has led to an increased interest in adhesive joints. Adhesive joints have some important advantages as compared to old-fashioned methods, eg. high strength, low weight and low thermal conductivity. Also, they are applicable to most material configurations and allows for dense joints. Since it is a new technique for joining two or more materials in advanced structures, such as chassis, new analysis methods for determining reliable design rules must be developed.

Much effort has already been put into understanding the mechanical aspects of adhesive joints. Both analytical, numerical and experimental studies have been performed.

In the paper by Chen et al. [1], a fracture analysis for a multi-material system with an interface crack was presented. For adhesive thickness much smaller than the length of the interface crack, a general formulation for the stress intensity factor was obtained using a dimensional analysis scheme. Avila-Pozos et al. [2] formulated an asymptotic model of an orthotropic, highly inhomogeneous layered structure. In this paper they developed a mathematical model for a thin three-dimensional layered structure. In this model, the adhesive layer is assumed infinitesimally thin and soft in comparison with upper and lower adherents. Ottosen and Olsson [3] have derived analytical solutions for an adhesive double lap joint, in which the adhesive behaves linear elastically, followed by either plastic hardening or softening. Softening plasticity approximates the behaviour of brittle adhesive such as conventional epoxy adhesives.

Finite element formulations of the problem have also been presented, with specially designed elements simulating the adhesive layer. In the paper by Andruet et al. [4], a special two- and three-dimensional element has been developed for stress and displacement analysis in adhesively bonded joints. Geometric nonlinearity is modelled, since large displacements often are observed in adhesive joints. Both two and three dimensional stress analyses of a single lap joint was presented. Ljungqvist [5] have also presented a paper based on a specially designed finite element. In the paper, various methods of simulating the adhesive were presented with the aim to be able to simulate the adhesive with a number of spring elements. Such elements were then used in a simulation of a truck cabin. Tvergaard and Hutchinson [6] have analysed the toughness of ductile adhesive joints. The paper includes a model to investigate the influence on joint toughness of both the elastic mismatches between the adhesive and the adherent and the residual stress in the adhesive layer. Also the effect of adhesive thickness was investigated.

Yang and Thouless [7] have investigated two different specimens, the T-peel specimen and the lap joint, experimentally as well as by finite elements. In their analysis they have considered cracked specimens, loaded in both mode I and mode II. The experimental measurements of the displacement versus load showed good agreement with the finite element results. Yang et al. [8], have performed a similar analysis as in [7]. The difference was that they used a different test specimen. They have also done some experiments on the adhesive shear properties from torsion tests. Guilleminet and Bistac [9] performed a wedge test on an adhesive joint. The aim of this study was to analyse the influence of the wedge indentation speed both on the failure energy and on the crack propagation rate.

In the present paper, an adhesive/adherent system consisting of toughened epoxy and steel will be investigated using the finite element method. A specially designed finite element to simulate eventual fracture of the system is introduced. The results of the simulations will be compared to the findings of others, in particular the results obtained by Stigh and Andersson [10,11].

2. Statement of the problem

The two different structures to be considered are the Double Cantilever Beam (DCB) and the lap joint, see figure 2.1. The two identical adherents of steel are joined together by an epoxy adhesive. The linear measures of the respective structure are shown in figure 2.2 and are, for the DCB specimen, chosen to correspond to the experiments performed by Stigh and Andersson [10,11]. The dimensions of the lap joint are chosen the same as for the DCB-specimen.

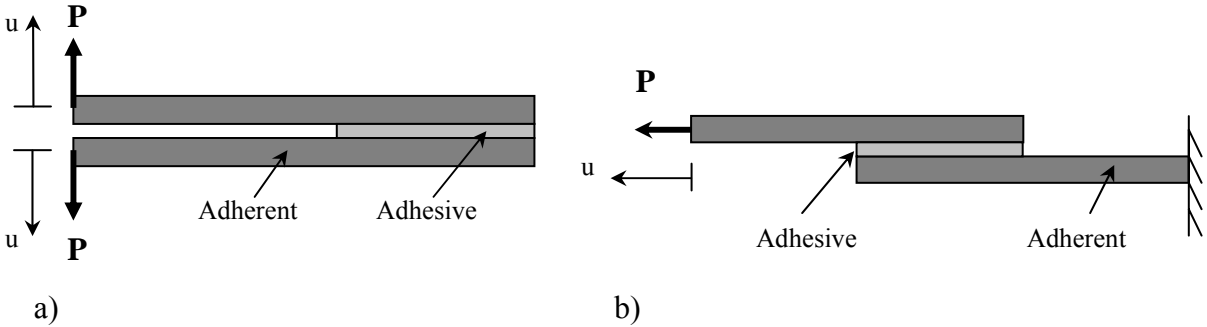


Figure 2.1. a) DCB-specimen, b) Lap joint

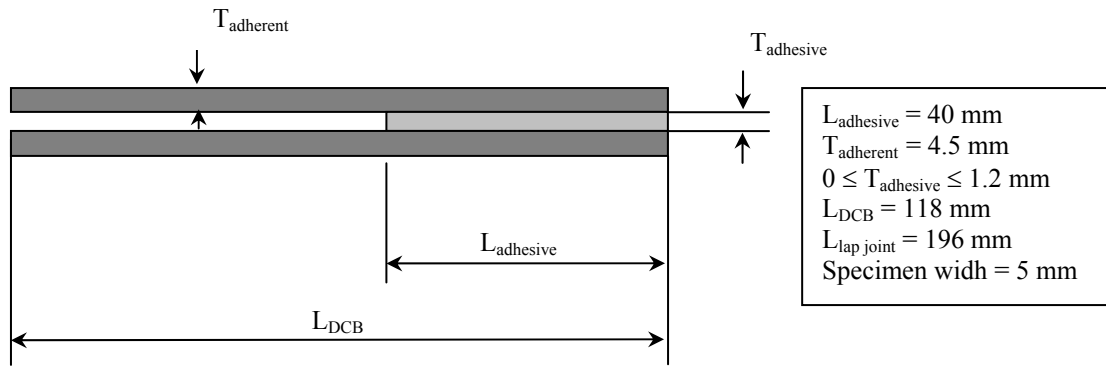
The structures are modelled by finite elements and plane conditions are assumed. The loading consists of a controlled displacement, u , of the outer end of the adherent according to figure 2.1. The force, P , is the reaction force at the outer end of the adherent. Since the DCB-specimen is symmetric in cases of no crack growth or crack growth along the symmetry line only the upper half needs to be modelled in these cases. A symmetry line is placed in the middle of the adhesive layer and along this line all displacements normal to it is set to zero.

For the adherent consisting of steel, a linear elastic material model is assumed. Stigh and Andersson [10,11] have shown that no plasticity in the adherent occurs due to the relatively small stresses at adhesive fracture. The material parameters for the adhesive are taken as the ones for the adhesive used by Stigh and Andersson [10,11]. The material parameters are given in table 2.1 where E denotes Youngs modulus, ν denotes Poissons ratio and σ_Y is the yield stress.

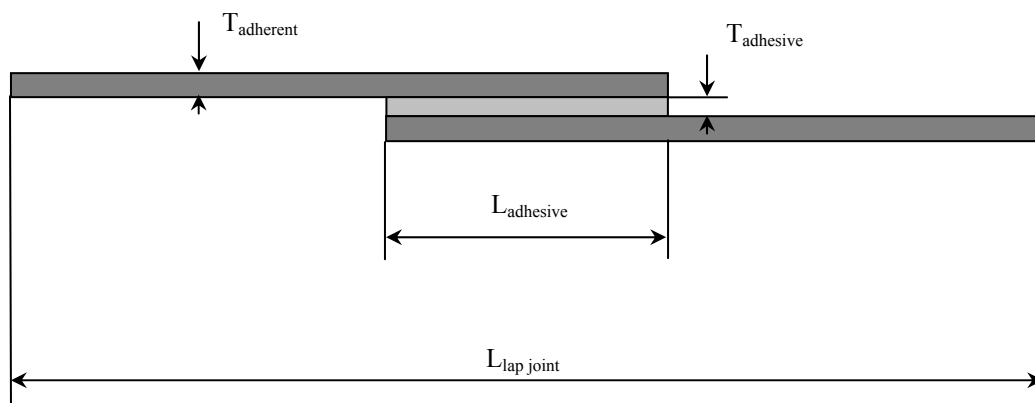
In order to be able to simulate crack growth at critical locations, cohesive zone elements were introduced along an assumed crack path as discussed below.

	Adhesive	Adherent
Material	Toughened epoxy Ciba Geigy XW 1044-3	Steel
E	$E_a = 2.2 \text{ GPa}$	$E_s = 206 \text{ Gpa}$
ν	$\nu_a = 0.4$	$\nu_s = 0.3$
σ_Y	$\sigma_{Ya} = 30 \text{ MPa}$	$\sigma_{Ys} > 450 \text{ MPa}$

Table 2.1. Material parameters for adhesive and adherent.



a) DCB-specimen.



b) Lap joint

Figure 2.2. Dimensions of the DCB-specimen and the lap joint.

3. Fracture modes

A crack in a material can develop in different ways and extend in different directions depending on the loading. In figure 3.1 the three different crack modes are displayed. It is the loading configuration, geometry and material characteristics that together determine the development at fracture. In the DCB-specimen mode I will be the dominating mode and in the lap joint mode II will dominate.

As the loading increases, a process zone develops ahead of the crack tip and a necessary prerequisite for the study of fracture is to form a model of the events in the process zone. Together with the choice of such a model, a proper fracture criterion must be chosen.

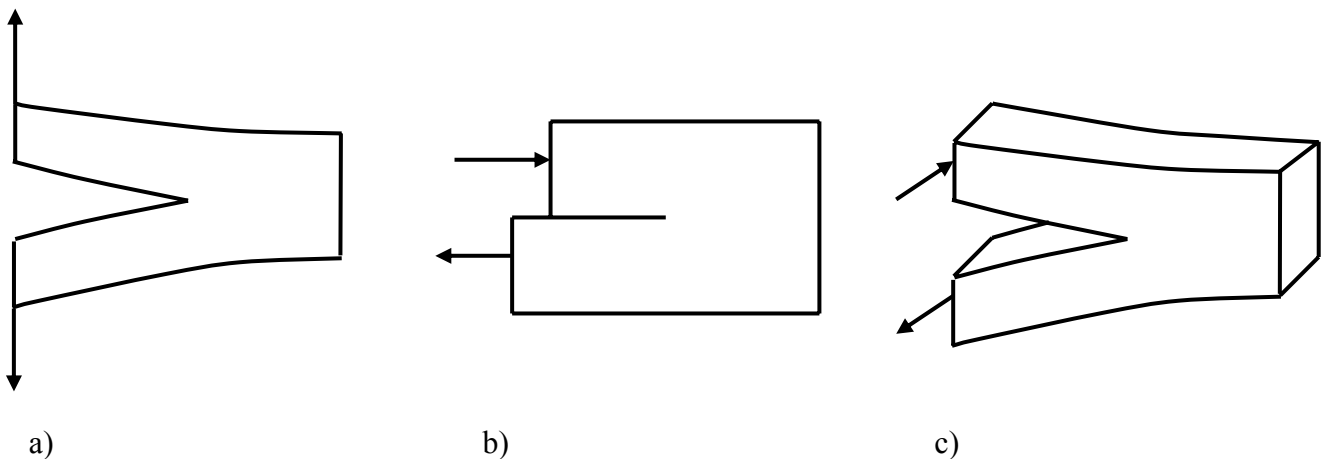


Figure 3.1. Description of different loading modes: a) Mode I, b) Mode II, c) Mode III

3.1 Process region description

The strip yield model [12] will be used to describe the state in the process region ahead of the crack tip. In this model, a prescribed relation between the crack opening displacement, $V_y(x)$, and the stress normal to the crack faces, i.e the closure stress, $\sigma(x)$, is assumed. As the displacement, $V_y(x)$, has reached a certain critical value, all material contact between upper and lower surfaces ceases and the crack starts to grow. Figure 3.2 illustrates mode I opening of the crack, but a similar situation applies to mode II and mode III.

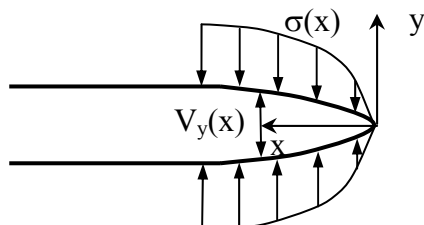


Figure 3.2. The strip yield model for mode I.

Two different stress-displacement laws describing the relation between $V_y(x)$ and $\sigma(x)$, referred to as model A and model B, will be considered in the present paper. The two different models mirror attempts to describe different experimental results. The first, model A, is the same as the one used by Stigh and Andersson [10,11] and the second one, model B, is the one used by Yang et al. [8].

The relations between $\sigma(x)$ and $V_y(x)$ in the case of mode I are shown in figure 3.3 for models A and B, respectively. The stress σ_Y denotes the largest stress that can be accommodated by the material and V_{yc} is the displacement at which the material contact ceases. The displacements V_{y1} , V_{y2} and V_{yc} specifies the appearance of the stress-displacement relation. The additional subscripts A and B refers to models A and B, respectively.

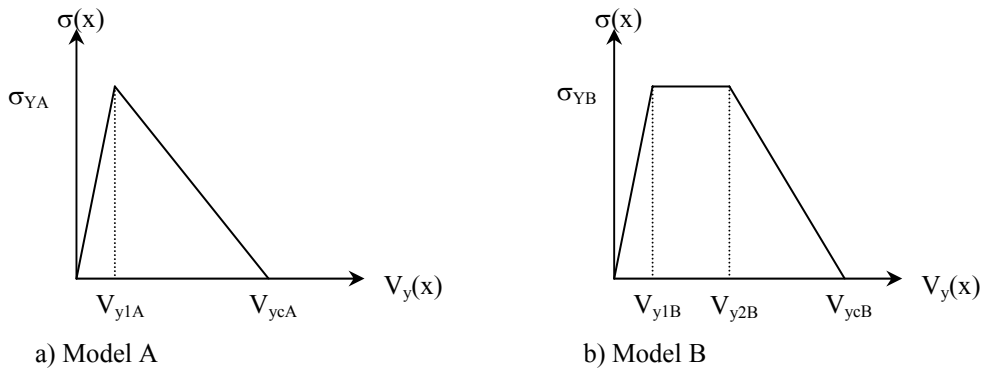


Figure 3.3. Relation between crack opening and stress in the two different models A and B.

Both in the DCB-specimen and in the lap joint shear stresses will also be present along the assumed crack path. Therefore a stress- displacement law for shear is also needed. Referring to Yang et al.[8] a stress-displacement law that accompanies shear can be developed for the two different models. Similar constitutive relations as the ones for mode I, figure 3.3, apply to mode II, in which case the parameters V_{y1} , V_{y2} , V_{yc} , σ_Y and V_y are replaced by V_{x1} , V_{x2} , V_{xc} , τ_Y and V_x where τ_Y is the shear yield stress.

3.2 Model A

From Stigh and Andersson [10,11] the following material data together with values of displacement parameters for model A were found:

$$\left\{ \begin{array}{l} E_a = 2.2 \text{ GPa} \\ \nu_a = 0.4 \\ \sigma_{YA} = 30 \text{ MPa} \\ J_c = 800 \text{ J/m}^2 \\ V_{y1A} = 1.3 \text{ } \mu\text{m} \\ V_{ycA} = 53 \text{ } \mu\text{m} \end{array} \right.$$

where J_c denotes the total fracture energy. From these data it is possible to calculate the work of normal separation per unit area of crack growth, Γ_{10} , in pure mode I load. The separation energy Γ_{10} equals the area beneath the V_y - σ curve in figure 3.4.

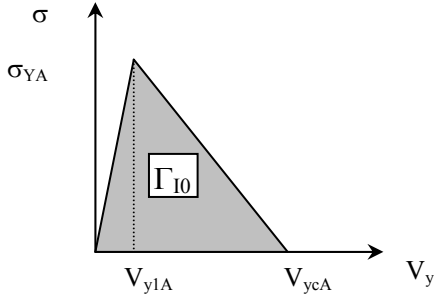


Figure 3.4. Work of separation, Γ_{I0} .

$$\Gamma_{I0} = 0.5 \{ \sigma_{YA} \cdot V_{ycA} + \sigma_{YA} \cdot (V_{ycA} - V_{y1A}) \} = 0.5 \cdot \sigma_{YA} \cdot V_{ycA} = 0.795 \text{kJm}^{-2} \quad (3.1)$$

In the first part of the analysis material model A, figure 3.3.a, will be used. The key parameters for normal stress in this model are V_{y1A} , V_{ycA} and σ_{YA} and the key parameters for shear stress is V_{x1A} , V_{xcA} and τ_{YA} . Test results presented by Yang et al. [8] show that the work of separation per unit area of crack growth is approximately five times larger for pure mode II than for pure mode I fracture. They have also showed that the peak shear stress is approximately 0.583 times the peak normal stress. Thus, from this

$$\Gamma_{II0} = 5 \cdot \Gamma_{I0} = 4.0 \text{kJm}^{-2} \quad (3.2)$$

$$\tau_{YA} = 0.583 \cdot \sigma_{YA} = 17.5 \text{MPa} \quad (3.3)$$

with Γ_{II0} denoting the work of shear separation per unit area of crack growth. From equations 3.2 and 3.3, the two shape parameters for mode-II fracture, V_{x1A} and V_{xcA} can be calculated. These shape parameters are given in table 3.1. The two different stress-separation laws of the material with proper relative critical shape parameters due to normal and shear stress is shown in figure 3.5.

Normal stress	Shear stress:
$\sigma_{YA} = 30 \text{MPa}$	$\tau_{YA} = 17.5 \text{MPa}$
$V_{y1A} = 1.3 \mu\text{m}$	$V_{x1A} = 11.2 \mu\text{m}$
$V_{ycA} = 53 \mu\text{m}$	$V_{xcA} = 457 \mu\text{m}$

Table 3.1. Shape parameters for model A.

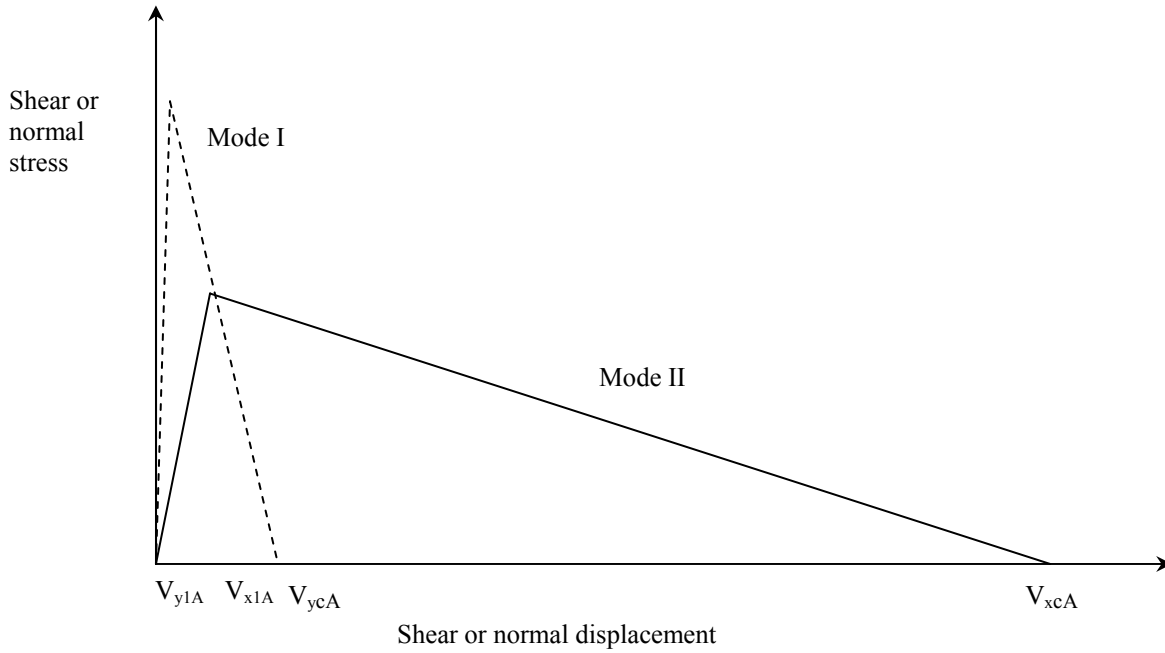


Figure 3.5. Opening (mode I) and shear (mode II) stress-separation laws for model A.

3.3 Model B

In the second part of the analysis model B will be employed, cf. figure 3.3.b. Yang et al. [8] have showed that the two key parameters for characterizing the fracture process are the interfacial toughnesses (Γ_{I0} or Γ_{II0}) and the peak stress (σ_{YB} or τ_{YB}). This means that the shape parameters, denoted V_{i1B} and V_{i2B} , with i equal to x or y , in this case, see figure 3.6, are of less importance and can be chosen arbitrary. In this analysis they are set to:

$$V_{i1B}/V_{icB} = 0.15 \quad (3.4)$$

$$V_{i2B}/V_{icB} = 0.5 \quad (3.5)$$

The maximum displacement V_{icB} , can easily be calculated from figure 3.6. From equations 3.4 and 3.5 the two shape parameters for each loading mode can be calculated, with the results shown in table 3.2.

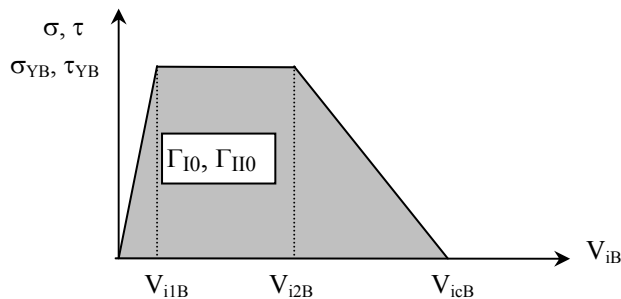


Figure 3.6. Work of separation, Γ_{I0} or Γ_{II0} . The subscript i equals to x or y .

Normal stress	Shear stress:
$\sigma_{YB} = 30 \text{ MPa}$	$\tau_{YB} = 17.5 \text{ MPa}$
$V_{ycB} = \frac{\Gamma_{I0}}{0.675 \cdot \sigma_Y} = 39.3 \text{ } \mu\text{m}$	$V_{xcB} = \frac{\Gamma_{I0}}{0.675 \cdot \tau_Y} = 339 \text{ } \mu\text{m}$
$V_{y1B} = 0.15 \cdot V_{ycB} = 5.89 \text{ } \mu\text{m}$	$V_{x1B} = 0.15 \cdot V_{xcB} = 50.8 \text{ } \mu\text{m}$
$V_{y2B} = 0.5 \cdot V_{ycB} = 19.6 \text{ } \mu\text{m}$	$V_{x2B} = 0.5 \cdot V_{xcB} = 169 \text{ } \mu\text{m}$

Table 3.2. Shape parameters for model B.

From these results figure 3.7 is constructed, in which the relative shape of the different behavior of the material in shear and normal stress can be seen.

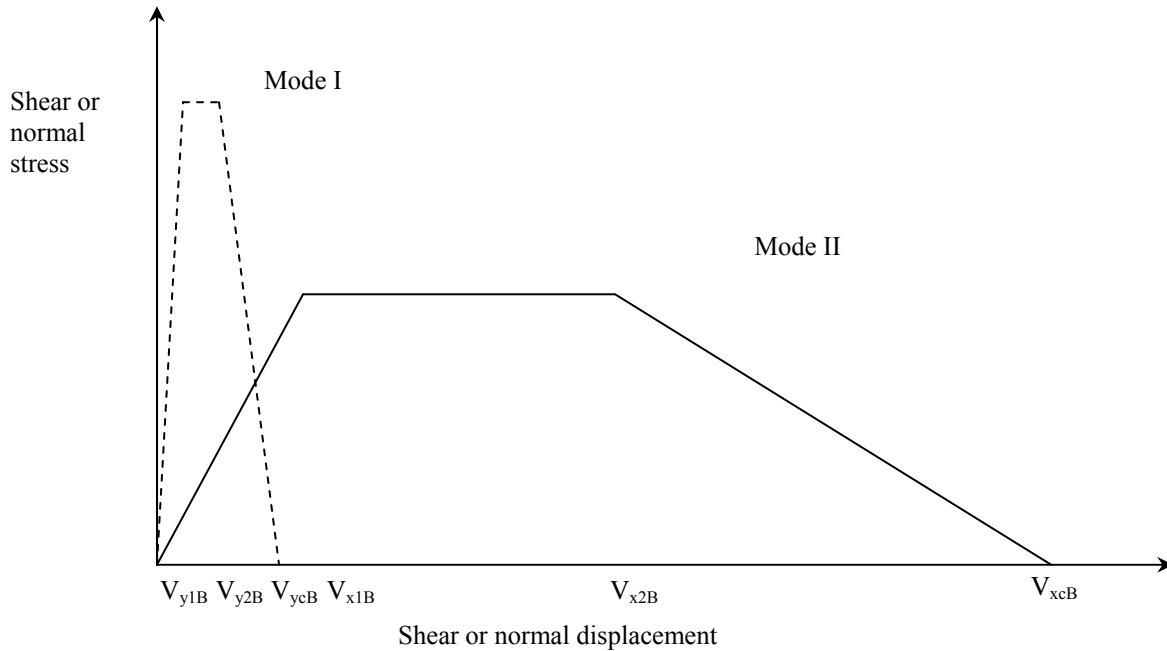


Figure 3.7. Opening (mode I) and shear (mode II) stress-separation laws for model B.

3.4 Failure criterion

Pure mode I fracture will occur when the fracture energy exceeds the critical value for mode I fracture, Γ_{Ic} . The same applies for mode II fracture:

$$\Gamma_{I0} = \Gamma_{Ic} \quad (3.6)$$

$$\Gamma_{II0} = \Gamma_{IIc} \quad (3.7)$$

In the general case the loading is a mixture of mode I and mode II and a special fracture criterion must be used. In this work, the fracture criterion according to Yang and Thouless [7]

is chosen. This criterion rests on the assumption that the total stress-separation work absorbed during fracture, G , can be separated into one opening (mode I) and one shear (mode II) component, G_I and G_{II} so that:

$$G = G_I + G_{II} \quad (3.8)$$

The two separate components can be calculated by integration of the mode I and mode II stress-separation curves, respectively, se figure 3.8:

$$G_I = \int_0^{V_y} \sigma(V_y) dV_y ; \quad G_{II} = \int_0^{V_x} \tau(V_x) dV_x \quad (3.9)$$

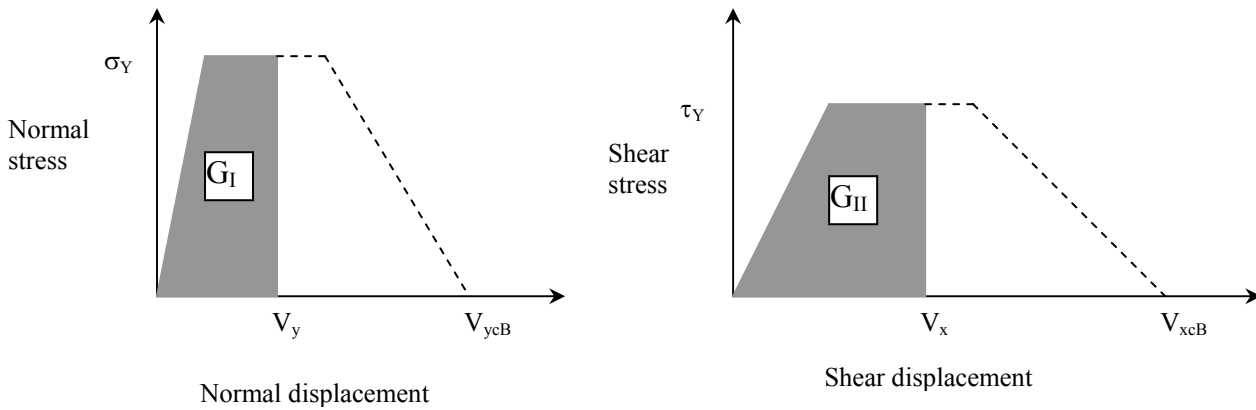


Figure 3.8. Schematic illustration of G_I and G_{II} .

The displacements, V_x and V_y , are not independent parameters. Rather, they evolve together as a natural result of the interplay between the deformation of the adherents and the two stress-separation laws. In order to determine the critical values of the two components of G , G_I^* and G_{II}^* , a failure criterion is required. This criterion is assumed to be [7]:

$$\frac{G_I^*}{\Gamma_{I0}} + \frac{G_{II}^*}{\Gamma_{II0}} = 1 \quad (3.10)$$

As loading progresses, the opening (V_y) and shear (V_x) displacement of the element are determined numerically, and G_I and G_{II} are then calculated from equations (3.9). When the failure criterion of equation (3.10) is met, the element fail and the crack advance.

4. Finite element implementation

In the analysis of the DCB-specimen and the lap joint the finite element method have been used, employing the general purpose code Abaqus 5.8 [13]. The two models are analysed in two dimensions using either plane strain or plane stress elements. Both element types were four noded. In figure 4.1 and figure 4.2, the mesh of the DCB-specimen can be seen. Each adherent consists of 2912 elements and the adhesive of 5970 elements in the case of adhesive thickness 0.2 mm. In order to minimize the computational time the elements are smaller in the most critical areas as seen in figure 4.2. In the adhesive layer the elements are even smaller in order to get a more accurate model. Figure 4.3 and figure 4.4 shows the mesh of the lap joint. The model is built according to the same principals as the mesh of the DCB-specimen.

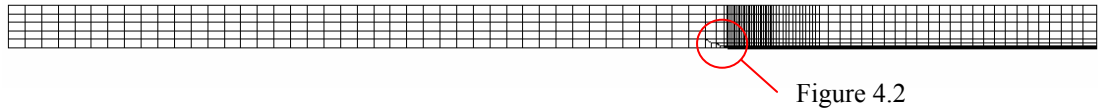


Figure 4.1. Finite element mesh of the DCB-specimen.

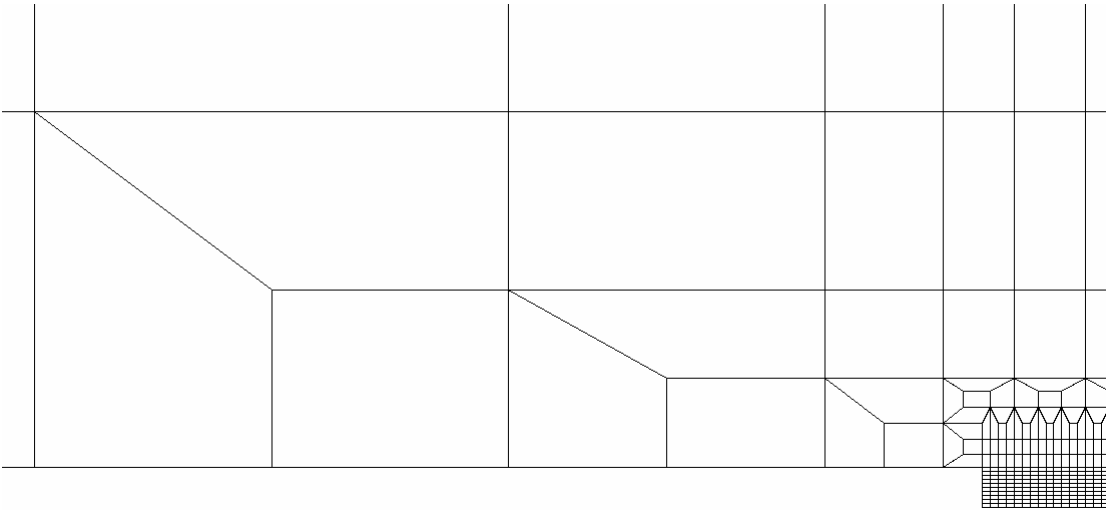


Figure 4.2. Enlargement of the enclosed area of the FE-mesh in figure 4.1.

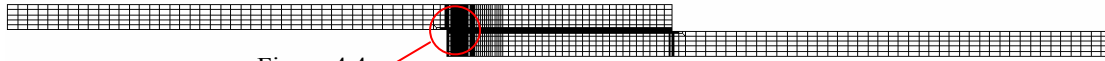


Figure 4.4

Figure 4.3. Finite element mesh of the lap joint.

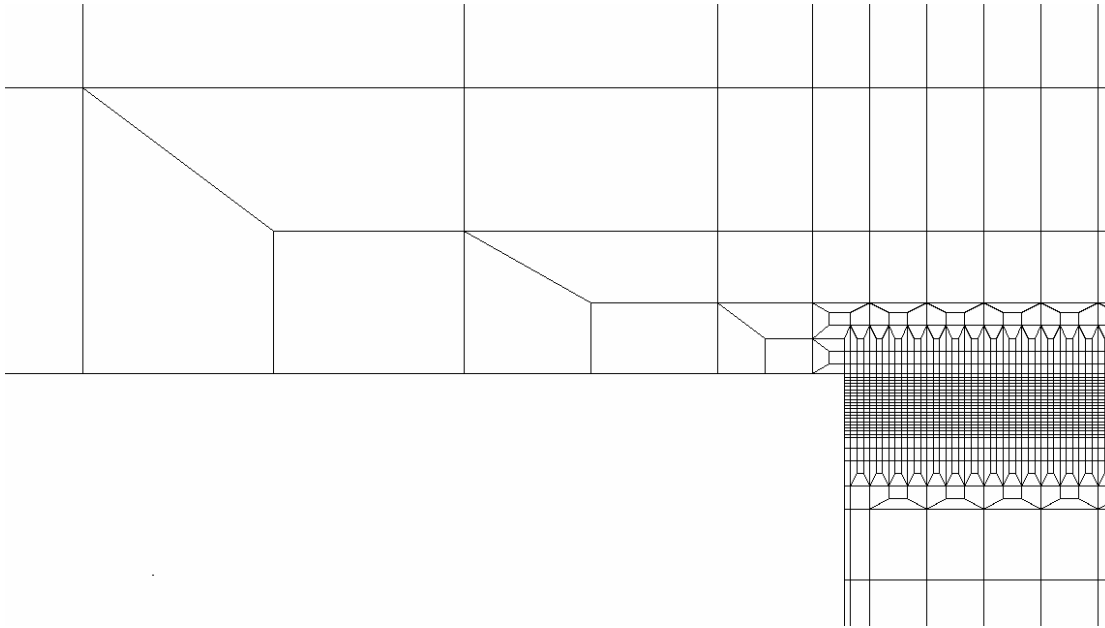


Figure 4.4. Enlargement of the enclosed area of the FE-mesh in figure 4.3.

4.1 Crack element

In this study, the fracture behaviour of different cracked configurations will be investigated. To that end a special crack element, to place along predetermined crack paths have been developed. The crack element is a further development of a similar element constructed by Andersson [14] to include the possibility to describe both material models A and B.

4.1.1 Crack element description

The crack element has four nodes, which are placed in couples and therefore the element will have the shape of a line. The node numbering of the element is according to figure 4.5. In order to simplify the calculations the displacements are transformed into a local coordinate system (x, y) and in this, the stiffness matrix, \mathbf{K} , and internal force vector, \mathbf{F}_{int} , are calculated and then transformed back to the global coordinate system (x', y') .

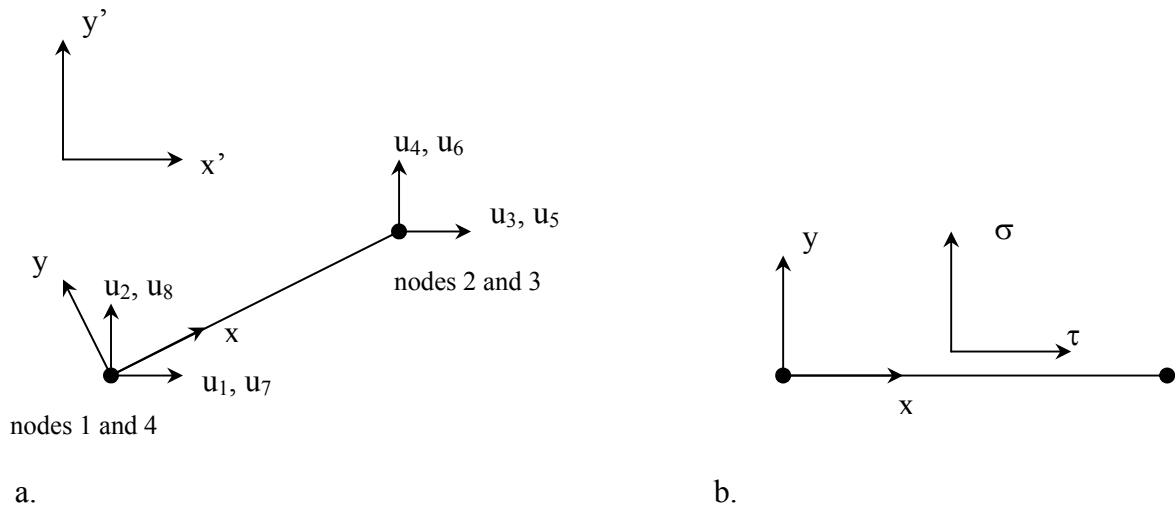


Figure 4.5. a. Crack element and its degrees of freedom, b. Stress definition

4.1.2 Element formulation

The vector \mathbf{a} contains all the displacement components (u_1 - u_8) for the element and the vector \mathbf{v} contains the relative displacements in the x and y directions at a point along the element. From these definitions, the following equations are obtained.

$$\mathbf{v} = \begin{bmatrix} v_x \\ v_y \end{bmatrix} = \mathbf{B}\mathbf{a} \quad (4.1)$$

where

$$\mathbf{B} = \mathbf{N}\mathbf{L} \quad (4.2)$$

The shape matrix \mathbf{N} is defined by

$$\mathbf{N} = \begin{bmatrix} N_1 & 0 & N_2 & 0 \\ 0 & N_1 & 0 & N_2 \end{bmatrix} \quad (4.3)$$

Linear shape functions have been employed according to:

$$N_1 = 1 - \frac{x}{L} \quad (4.4)$$

$$N_2 = \frac{x}{L} \quad (4.5)$$

where L is the element length, N_1 relates to nodes 1 and 4 and N_2 to nodes 2 and 3.

The \mathbf{L} matrix equals

$$\mathbf{L} = \begin{bmatrix} -1 & 0 & 0 & 0 & 0 & 0 & 1 & 0 \\ 0 & -1 & 0 & 0 & 0 & 0 & 0 & 1 \\ 0 & 0 & -1 & 0 & 1 & 0 & 0 & 0 \\ 0 & 0 & 0 & -1 & 0 & 1 & 0 & 0 \end{bmatrix} \quad (4.6)$$

Define k_y as the slope of the normal stress curve and k_x as the slope of the shear stress curve. With these definitions a constitutive matrix, \mathbf{D} , can be formed:

$$\mathbf{D} = \begin{bmatrix} k_x & 0 \\ 0 & k_y \end{bmatrix} \quad (4.7)$$

The element stiffness and the internal forces can be calculated from [13]:

$$\mathbf{K}_e = b \int_0^L \mathbf{B}^T \mathbf{D} \mathbf{B} dx \quad (4.8)$$

$$\mathbf{F}_{\text{int}} = b \int_0^L \mathbf{B}^T \boldsymbol{\sigma} dx \quad (4.9)$$

where b is the element thickness and $\boldsymbol{\sigma}$ is the vector containing the stresses at the surface of the element according to figure 4.5.b:

$$\boldsymbol{\sigma} = \begin{bmatrix} \tau \\ \sigma \end{bmatrix} \quad (4.9)$$

The integrations are performed numerically by a three point Gauss integration scheme according to Ottosen and Petersson [15].

5. Analysis of uncracked specimens

In this chapter the finite element model is used for stress analysis in specimens prior to failure. The specimens are assumed to be free of any initial cracks or other defects. The models are two dimensional and four noded plane stress elements were used. The idea behind these runs is to determine critical areas of the joint, in which the highest stresses occurs, and from that reason where the highest probability for crack initiation is located. To get this rough estimate of critical areas where cracks may evolve, a prescribed displacement at the tip of the adherents is applied, se figure 2.1.

5.1 Stress distribution in the DCB-specimen

5.1.1 Stress analysis

In order to rationalise the calculations a symmetry line in the middle of the adhesive is created. In this first model an adhesive thickness of 0.2 mm is used, which correspond to the thickness used by Stigh and Andersson [10,11]. The total number of nodes in the finite element model is 9280 and the number of elements is 8882. In order to get a high accuracy in the adhesive layer, it is modelled with 6000 elements, with the layer thickness of 10 elements. The material parameters are also chosen according to [10,11]. The elastic material constants are given in table 2.1. To simplify the model the bonding between the adherent and the adhesive is assumed to be ideal, which means that no debonding occurs at the interface.

5.1.2 Boundary conditions

The DCB geometry is shown in figure 2.1, from which it can be seen that the specimen is constrained in the second degree of freedom (2-direction) along its symmetry line. The node at the end furthest from the point of load application of the adhesive is also constrained in the first degree of freedom. The loading is displacement controlled which means that the node at the tip of the adherent has a prescribed maximum displacement of 0.3 mm. This displacement is chosen arbitrary since the scope of the investigation is to determine areas of possible crack initiation.

5.1.3 Results

In figures 5.1-5.8 the distributions of the different stress in the DCB-specimen are shown. The stresses around the adhesive/adherent interface are especially interesting and therefore an enlarged picture of this area is included for each stress distribution.

5.1.3.1 The von Mises equivalent stress.

The von Mises equivalent stress distribution is shown in figures 5.1 and 5.2. It is of special interest since one might assume that the area with the highest effective stress is the most critical one. From this stress distribution, one can see that the highest effective stress in the adherent, about 40 MPa, is located at a point directly above the start of the adhesive layer. One can also see that the stress falls as one move away from this area, both in positive and negative 1-direction.

Since the adhesive is more sensitive to normal stress than shear stress [7], the von Mises equivalent stress distribution is not enough in order to determine the most critical area in the adhesive layer and therefore all stress components should be analysed each by each.

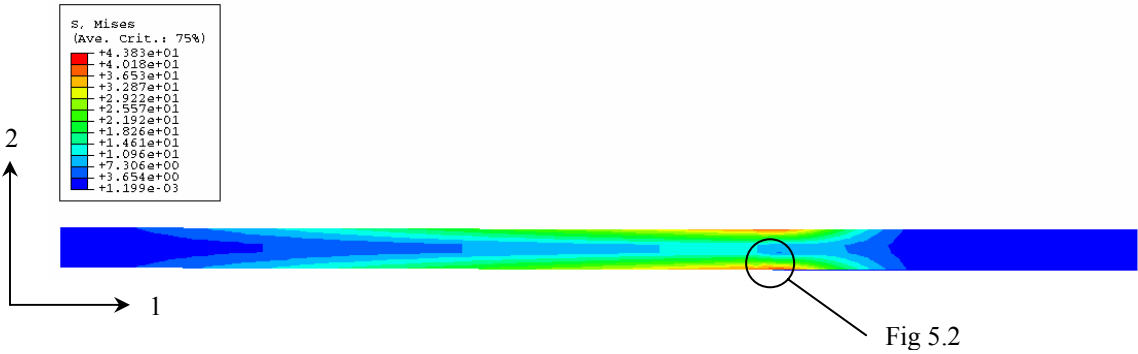


Figure 5.1. DCB-specimen, von Mises stress distribution.

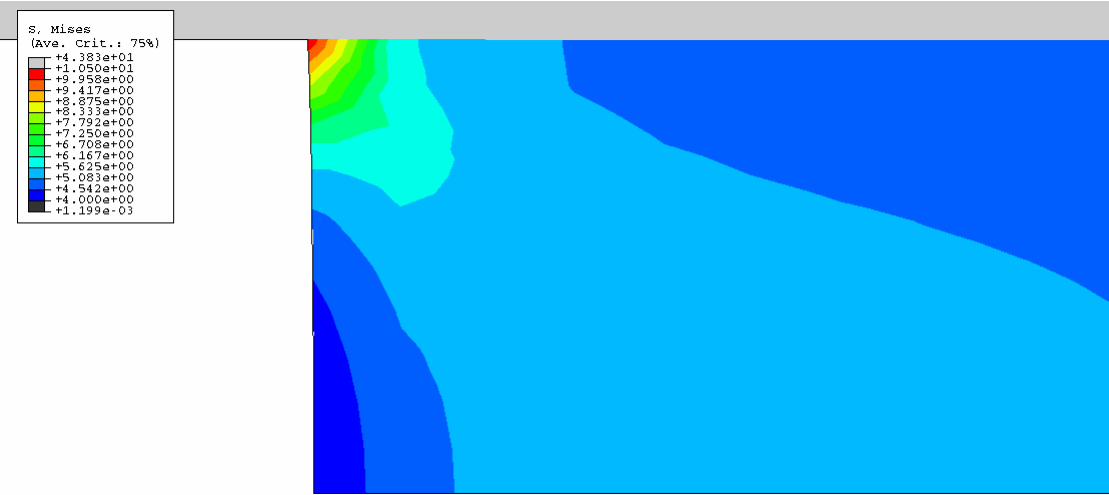


Figure 5.2. Magnification of the adhesive, von Mises stress distribution.

5.1.3.2 Normal stress in the 1-direction

The normal stress distribution in the 1-direction, se figure 5.3, is similar to the von Mises distribution, except that the stresses have different sign on the upper and lower surface. That is because the von Mises equivalent stress do not account for the sign of the different stresses. The highest stress in the adherent is approximately 45 MPa on the lower surface and -45 MPa at the upper surface.

One can see from figure 5.4 that the largest stress in the adhesive is at the interface between the adhesive and the adherent, approximately 4 MPa.

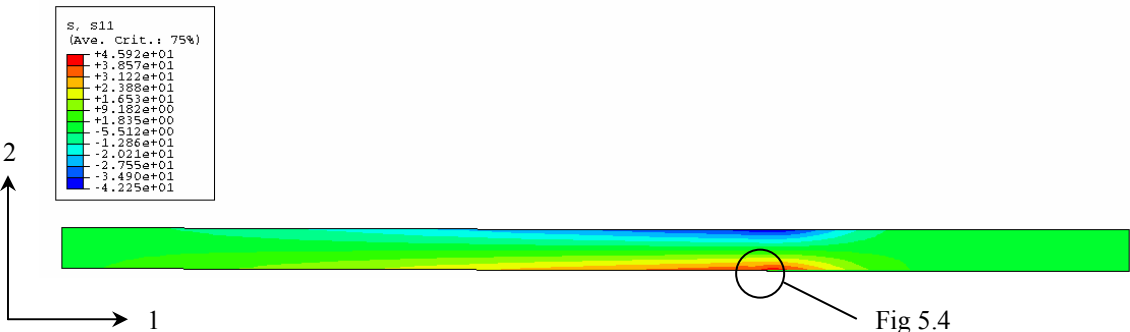


Figure 5.3. DCB-specimen, normal stress distribution in the 1-direction.

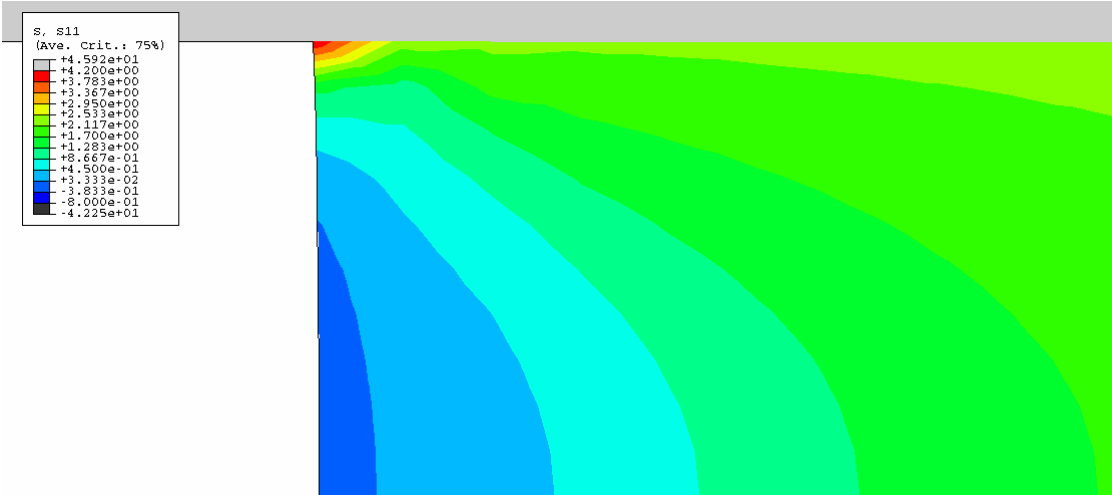


Figure 5.4. Magnification of the adhesive, normal stress distribution in the 1-direction.

5.1.3.3 Normal stress in the 2-direction

The normal stress in the 2-direction, see figure 5.5, is low in the construction except near the tip of the adhesive/adherent interface in the adherent. The stress at this point is approximately 6 MPa.

In figure 5.6 one can see that the highest stress in the 2-direction in the adhesive layer occurs at the interface at the top of the adhesive. The stress at this point is approximately 10 MPa.

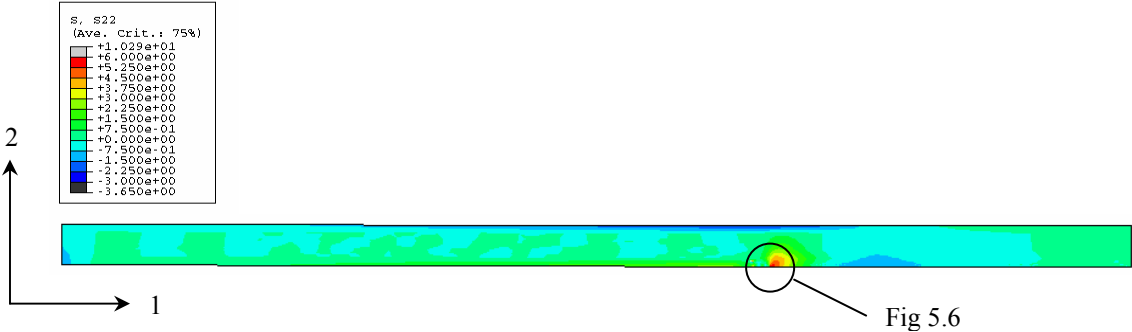


Fig 5.5. DCB-specimen, normal stress distribution in the 2-direction.

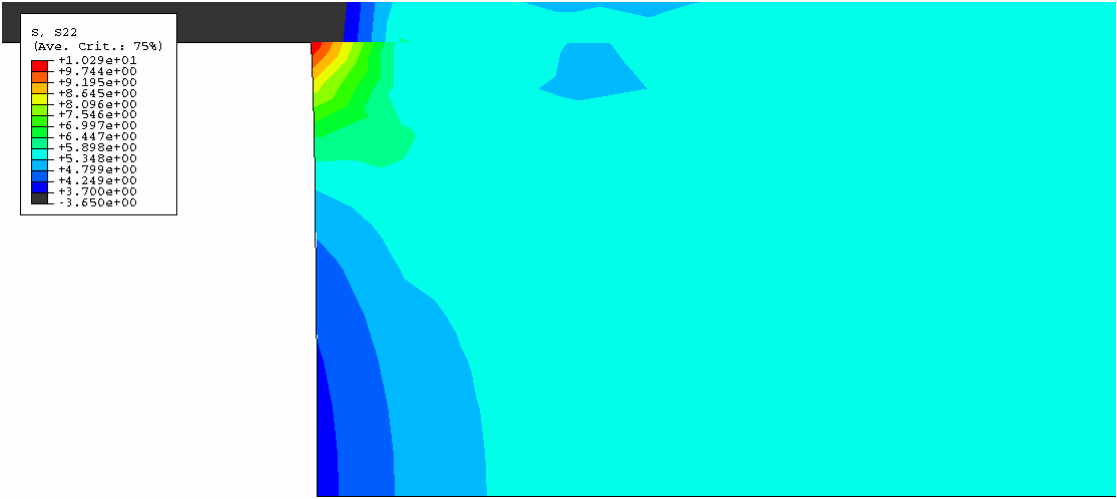


Figure 5.6. Magnification of the adhesive, normal stress distribution in the 2-direction.

5.1.3.4 Shear stress distribution

From figure 5.7 one can see that the shear stress in the adherent is low, the highest value is approximately 6 MPa at the centre of the adherent above the adhesive layer.

From the shear stress distribution in figure 5.8 one can see that the lowest shear stress in the adhesive occurs at the adhesive/adherent interface, this stress is approximately -3 MPa. One can also see that the shear stress at the centre of the adhesive (along the symmetry line) is equal to zero.

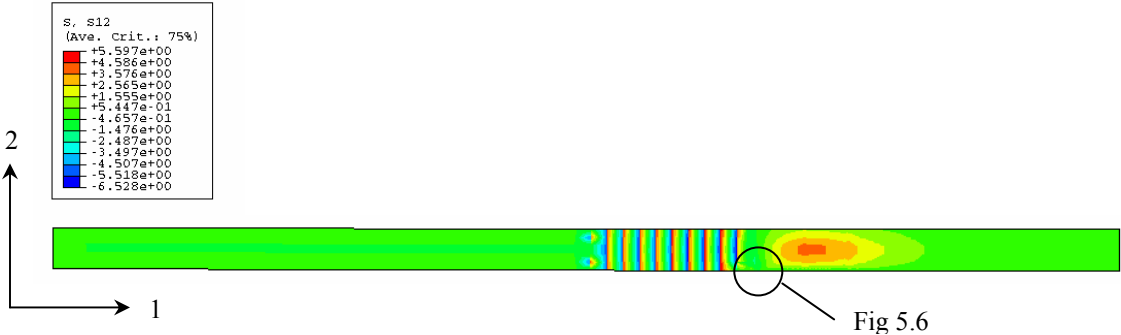


Figure 5.7. DCB-specimen, shear stress distribution.

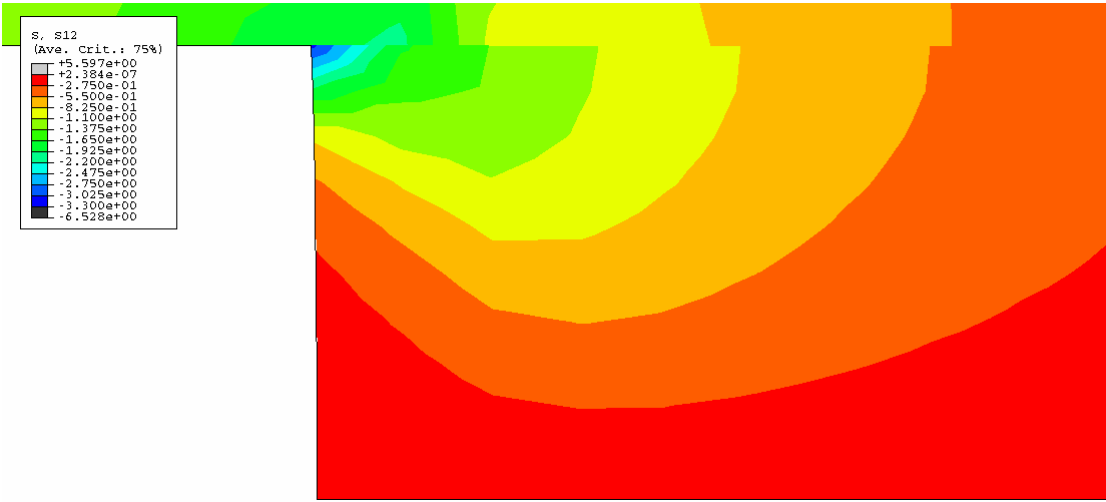


Figure 5.8. Magnification of the adhesive, shear stress distribution.

5.2 Stress distributions in the lap joint

5.2.1 Stress analysis

The material description and the adhesive thickness are the same as in the DCB-specimen analysis. The same assumptions of debonding also hold. The finite element model consists of 17986 nodes and 17787 elements. In order to get a high accuracy in the adhesive layer, it is modelled with 12000 elements, with the thickness of 20 elements. The large number of elements depend on that no symmetry line exists and therefore the whole model of the lap joint is modelled.

5.2.2 Boundary conditions

The geometry of the lap joint can be seen from figure 2.1. It indicates that all nodes at the right end of the lower adherent are fully constraint, which means that all degrees of freedoms are constrained at this end. The model is displacement controlled which means that all nodes on the left end of the upper adherent have a prescribed displacement of 0.1 mm in the 1-direction. The displacement is chosen arbitrary to give a picture of most critical areas in the model.

5.2.3 Results

Figures 5.9-5.16, show the stress distribution of the lap joint for different stress components. The stresses around the adhesive/adherent interface are especially interesting, therefore an enlarged picture of this area is taken for all the different stress distributions. From this the stresses in the adhesive layer can be studied more precisely.

5.2.3.1 The von Mises equivalent stress.

The von Mises equivalent stress distribution, see figure 5.9, shows that the highest effective stresses in the adherent is located near the beginning of the adhesive layer. The highest stress in this area is approximately 220 MPa. The enlarged area in figure 5.10 shows that the stress falls along the adhesive layer. Large stresses also occur at the end of the adherent, with a maximum of approximately 130 MPa.

The enhanced figure 5.10, also shows that the largest effective stress in the adhesive occurs at the tip of the adherent/adhesive interface. This stress is approximately 50 MPa.

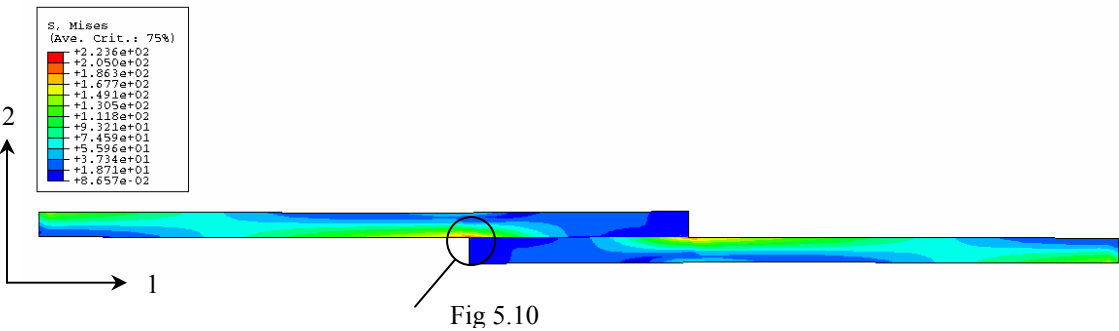


Figure 5.9. Lap joint, von Mises stress distribution.

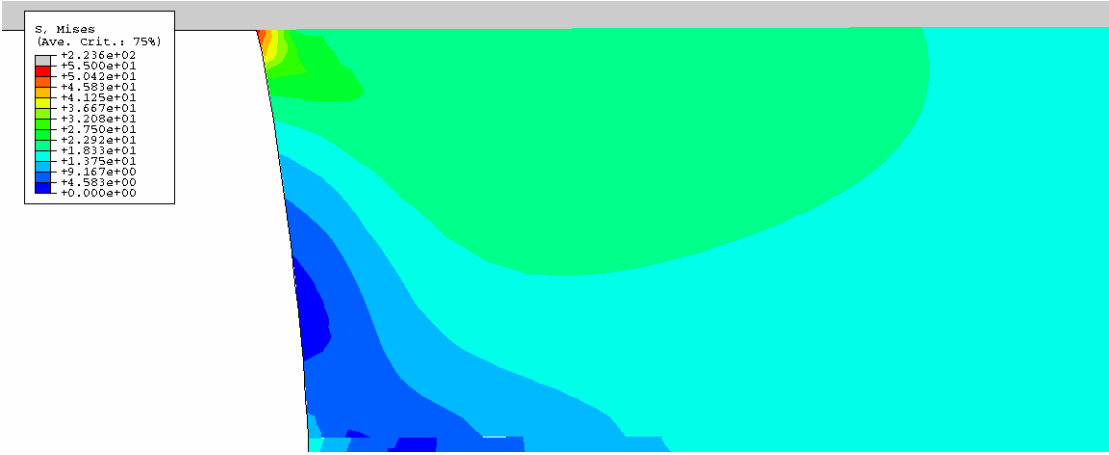


Figure 5.10. Magnification of the adhesive, von Mises stress distribution.

5.2.3.2 Normal stress in the 1-direction

The stress distribution in the 1-direction, see figure 5.11, shows that the highest stress in the adherent occurs at the same place as in the von Mises stress distribution. In this area, the highest stress is approximately 250 MPa.

Figure 5.12, shows that the highest stress in the 1-direction in the adhesive occurs at the interface between the two materials. It is located somewhat behind the tip of the adhesive layer and is approximately 20 MPa. One can note that the largest stress in this direction is not located at the same position as for the von Mises stress distribution.

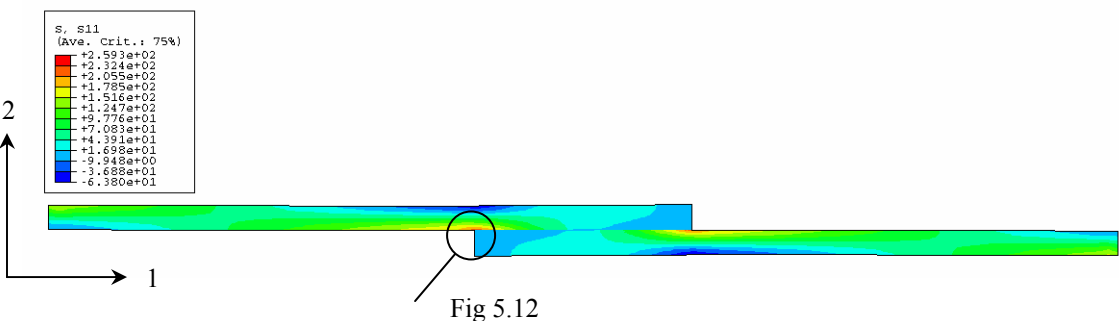


Figure 5.11. Lap joint, normal stress distribution in the 1-direction.

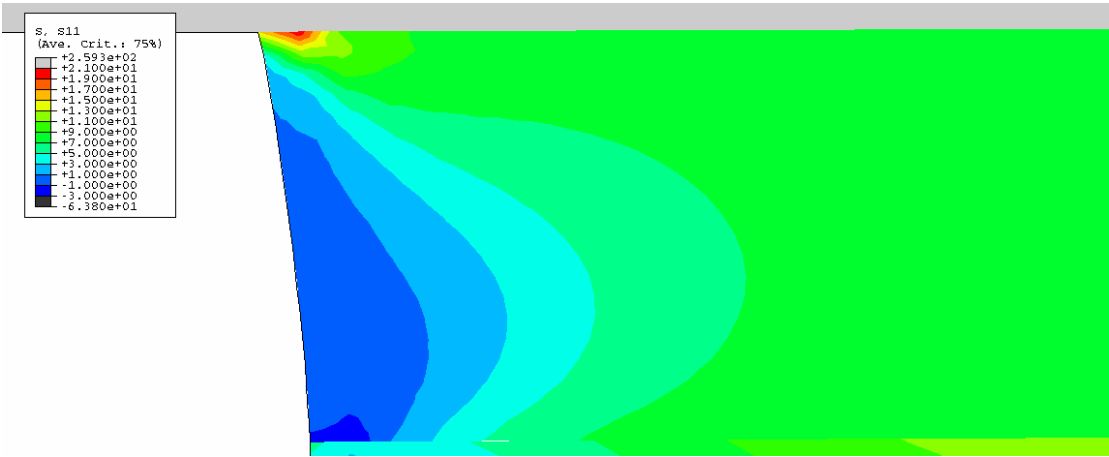


Figure 5.12. Magnification of the adhesive, normal stress distribution in the 1-direction.

5.2.3.3 Normal stress in the 2-direction

The normal stress in the 2-direction is much smaller than in the 1-direction, see figure 5.13. The highest stress in the adherent is approximately 30 MPa and is located at the end of the adherent. Near the adhesive layer, the stress is as low as 10 MPa, approximately.

In the adhesive layer, see figure 5.14, the largest stress is approximately 50 MPa and located at the upper tip of the adhesive layer. In the lowest part of the tip the lowest stresses occur, approximately -10 MPa, i.e. a compressive stress.

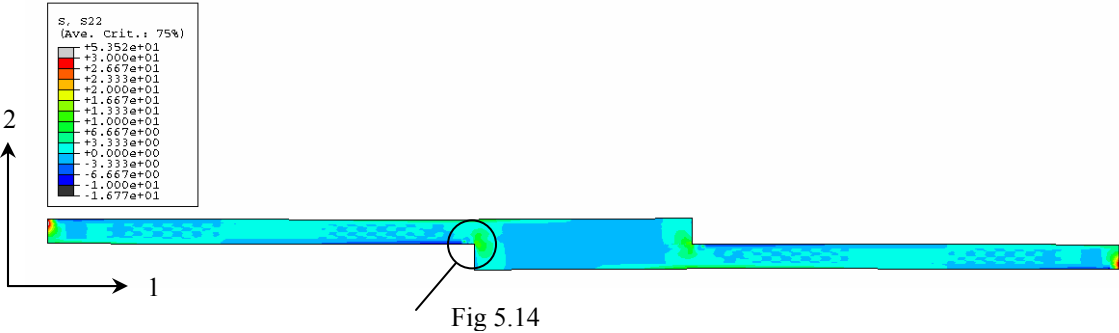


Figure 5.13. Lap joint, normal stress distribution in the 2-direction.

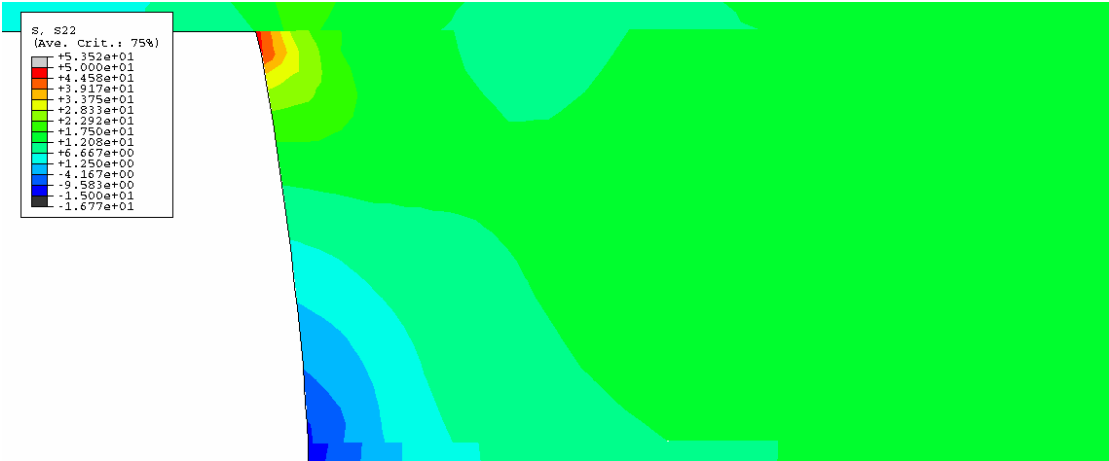


Figure 5.14. Magnification of the adhesive, normal stress distribution in the 2-direction.

5.2.3.4 Shear stress

The largest positive shear stress in the adherent is located above the adhesive in the centre of the adherents are seen from figure 5.15. This stress is approximately 10 MPa. The largest negative shear stress is located at the end of the adherent and is approximately -30 MPa.

In the adhesive layer the largest negative shear stress is located at the tip of the adhesive, see figure 6.8. This stress is approximately -25 MPa.

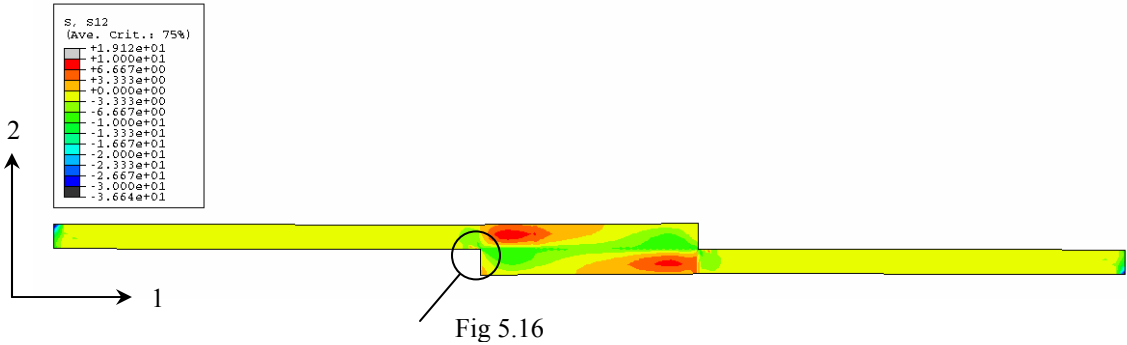


Figure 5.15. Lap joint, shear stress distribution.

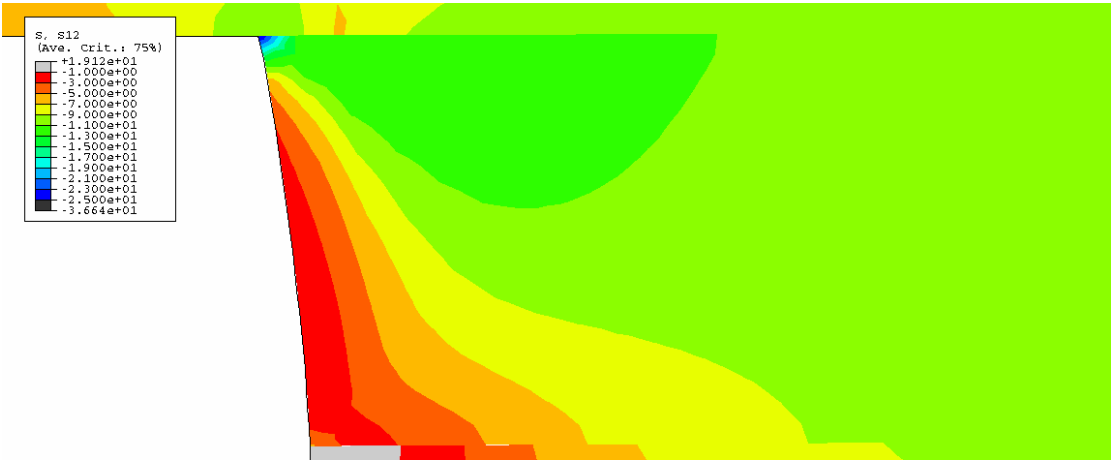


Figure 5.16. Magnification of the adhesive, shear stress distribution.

5.3 Crack path prediction

From the different stress distributions it is possible to predict where the most critical areas are located. Both specimens show similar behaviour.

In the adhesive, the most critical area is at the tip of the adhesive layer, close to the interface between adhesive and adherent. Therefore, one predetermined crack path will be chosen along the adhesive/adherent interface. Furthermore, a predetermined crack path along the centre line of the adhesive will be investigated.

For the adherent the most critical areas are directly above the tip of the adhesive layer, in this area the largest stresses occur. By studying the different stress distribution one can see that the stress in this area is a positive stress and therefore dangerous for crack propagation. In this thesis, however, only cracks in the adhesive and in the interface between the adhesive/adherent will be analysed, since it is assumed that the strength of the adhesive is much lower than that of the adherent.

6. Fracture analysis of the DCB-specimen

In the analysis, two different pre-determined crack paths have been investigated. Along these pre-determined paths cohesive crack elements were placed. The first crack path is along the symmetry line in the adhesive layer, see figure 6.1.a, and the other is in the interface between the adhesive and the adherent, see figure 6.1.b. A number of different adhesive thicknesses have been studied in order to determine how the adhesive thicknesses influence the global behaviour of the joint. Also the influence of the choice of plane stress and plane strain modelling is investigated.

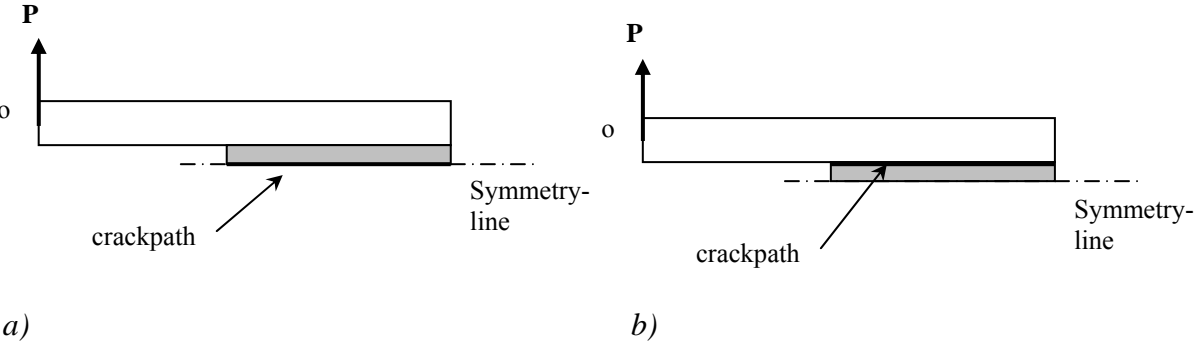


Figure 6.1. Crackpaths in the DCB-specimen

6.1 Comparison between plane stress and plane strain state

The influence of choice of plane state of the DCB-specimen, plane stress or plane strain elements, for the adherents and adhesives has been investigated. The adhesive thickness is 0.2 mm and the crack elements are placed along the symmetry line according to figure 6.1.a. The analysis is displacement controlled, the upper end of the adherent have a prescribed displacement of maximum 4.0 mm at point o in figure 6.1, giving a maximum separation of the adherents of 8.0 mm. The analysis is performed in 40 equal steps and the reaction force at point o in figure 6.1 is plotted against the displacement at this point, see figure 6.2.

The calculations in plane strain could be pursued to an adhesive separation of 7.8 mm before numerical divergence occurred. The plane stress calculation was interrupted at adhesive separation 8.0 mm.

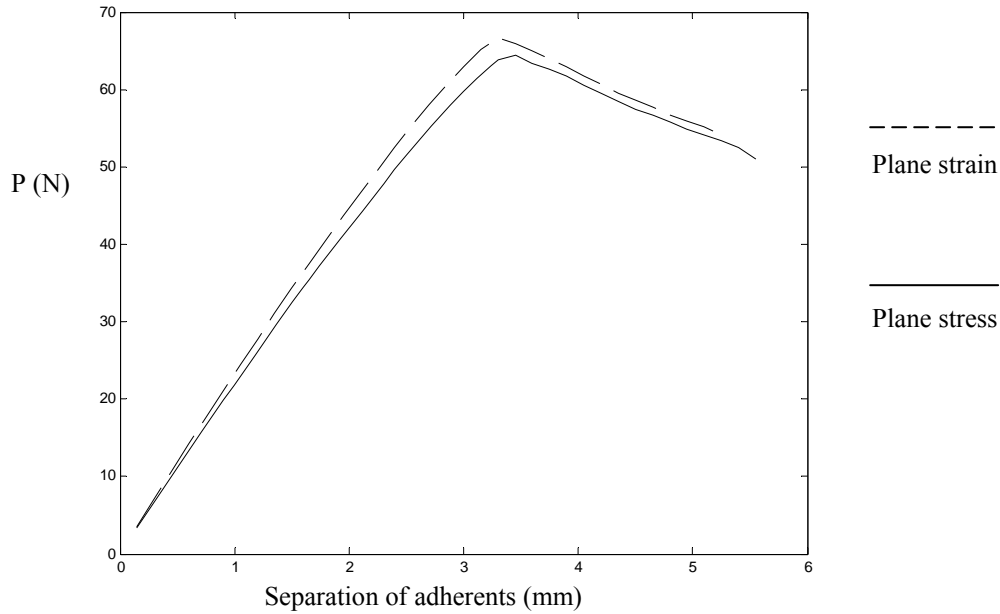


Figure 6.2. Plane stress and plane strain simulations, force vs. adhesive separation.

As seen in figure 6.2, the differences in results from the two different types of plane elements are small. The plane strain elements make the model stiffer than the plane stress elements and therefore gives a higher maximum force. The maximum of the curves indicates the points where total relaxation of the outermost crack element occurs. As seen from figure 6.2, the difference in force at this point is only 3 %. The results are in good agreement with the ones presented by Yang et al. [8]. They have also showed that plane stress elements show better agreement with experimental results than plane strain elements. The plane strain elements have a tendency to overestimate the stiffness. Therefore, plane stress elements will be used in the following part of the analysis for both the DCB-specimen and the lap joint.

6.2 Influence of choice of stress-separation law

A comparison of the results, using model A and model B, has been performed. The crack elements are placed along the symmetry line and plane stress elements are used for both the adherent and the adhesive. Adhesive thickness is 0.2 mm. The analysis is displacement controlled, the end of the adherent has a prescribed displacement and the force is the reaction force at this point. The analysis is performed in 40 steps of the same length, with the maximum separation of the adherents 8.0 mm. Figure 6.3 shows the separation of the adherents as function of the reaction force at the same point for the two models.

From figure 6.3 one can see that model B has a lower maximum value of the force than model A. The top of the curve coincides with the point when the first crack element is totally relaxed, i.e. as $V_{iy} = V_{iyc}$, where i denotes A or B, cf. figure 3.3. When this first element relaxes the reaction force P decreases as the applied displacement continues to increase. Also, model B predicts earlier separation than model A.

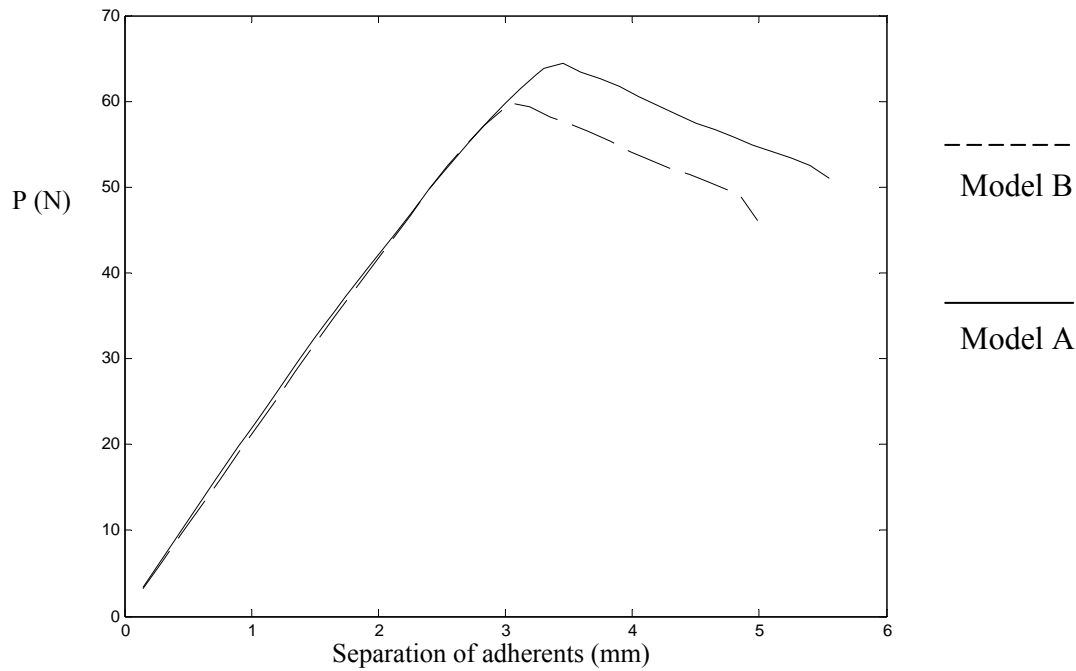


Figure 6.3. Force versus separation of the adherents for the both models.

The vertical displacement (V_{iy}) as a function of position along the adhesive layer in the x-direction prior to crack growth was also studied for the two models A and B. In this study, the vertical displacement at the left end of the adherent was chosen to be 0.3 mm. The placement of the x-axis can be seen in figure 6.4.

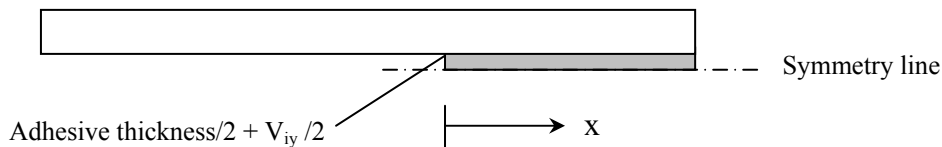


Figure 6.4. Description of the test configuration.

From figure 6.5 it is seen that the adhesive is separated at the end of the layer at $x = 0$. With increasing x , the separation decreases to a point where it changes to be a compression of the adhesive. This compression reaches a minimum value and increases after this point. This applies to both model A and model B. The difference in behavior can be seen in figure 6.5. Model A has a higher stiffness and is therefore less separated at $x = 0$ than model B. This difference in stiffness also has the effect that a smaller part of the adhesive is compressed in the case where model A is used. The obtained results are in good agreement with the ones obtained by Stigh and Andersson [10,11].

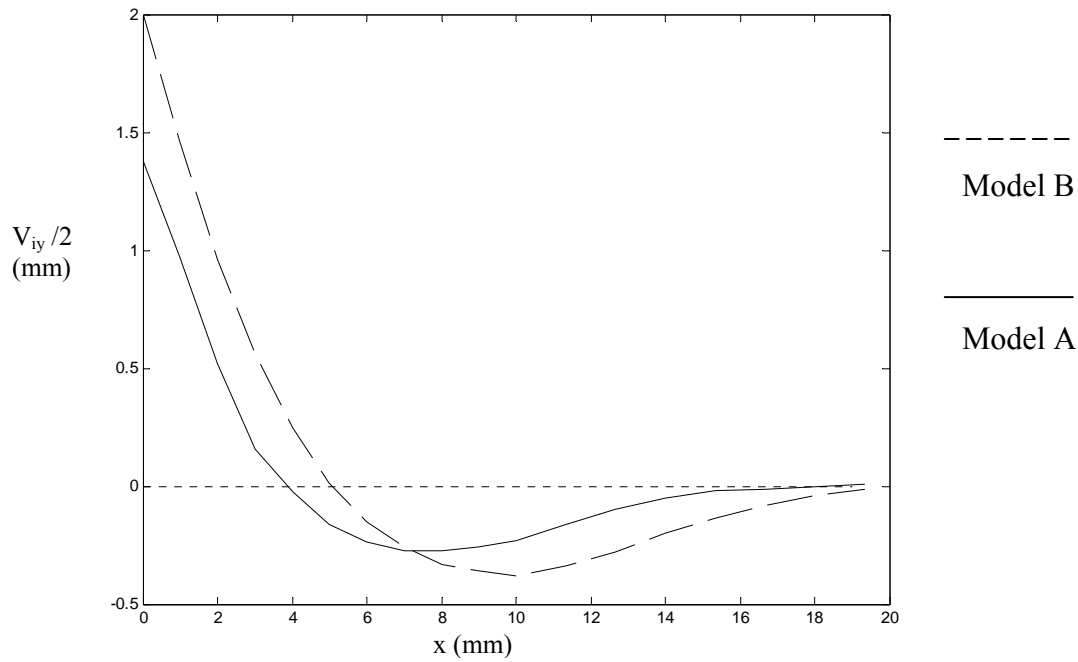


Figure 6.5. Elongation of adhesive along the specimen.

As a result of the analysis the crack length as a function of separation of the adherents is also obtained as the displacement at the end of the adherent is increased, see figure 6.6.

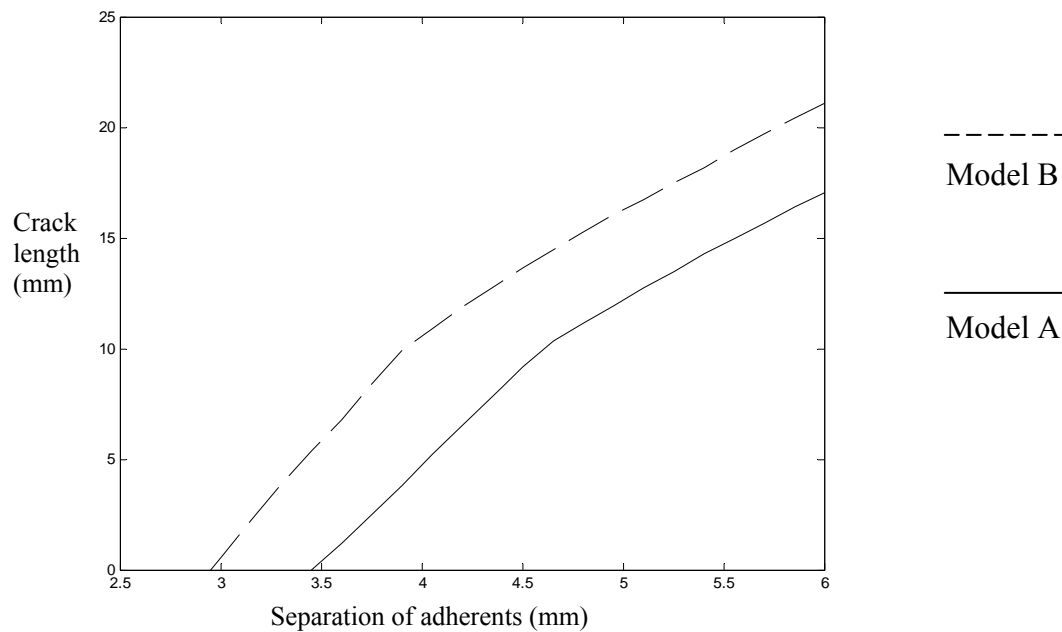


Figure 6.6. Crack length as a function of separation of the adherents.

As seen from figure 6.6, model B starts to crack at a smaller separation of the adherents as compared to model A. One can also see that the shape of the two curves is similar, resulting in that at a certain displacement between the adherents (beyond the crack initiation point) model B predicts a longer crack than model A.

6.3 Crack path along symmetry line, variable thickness of the adhesive

A similar analysis as discussed in chapter 6.2 was performed with two more adhesive thicknesses, 0 mm and 0.04 mm. The force versus separation of the loading points was studied. The obtained results were almost identical to the ones obtained in the previous analysis with an adhesive thickness of 0.2 mm. This leads to the conclusion that the adhesive thickness does not influence the global behavior of the DCB-specimen assuming a crack along the symmetry line.

6.4 Crack path along the interface, variable thickness of the adhesive

In this part of the analysis of the DCB-specimen, the crack elements are placed at the interface between the adhesive and the adherent, see figure 6.1.b. Four different thicknesses were analysed, 0, 0.04, 0.2 and 1.2 mm. The analysis is performed in the same manner as the analysis for a crack along the symmetry line discussed in chapter 6.2. When the crack is placed along the interface one could assume that it would start to grow at a smaller separation of the adherents than a crack along the symmetry line. This is because no mode-II loading is present in the case of a crack along the symmetry line, but in the case of a crack along the interface, such loading occurs.

When analyzing the first three thicknesses no differences between a crack along the interface as compared to a crack along the symmetry line could be seen. To confirm this, an additional analysis with a very large adhesive thickness of 1.2 mm was performed. In this analysis, one could notice a very small increase in maximum force before crack initiation. This increase was, however, only about 1 % as compared to the results from chapter 6.2. One could also see that crack initiation occurred somewhat earlier than for the smaller thicknesses. This difference was, however, neglect able.

The explanation why the difference between the interface crack and the crack along the symmetry line is so small is that the contribution of mode II is very small in the DCB-specimen. As the adhesive thickness increases the contribution from mode II increases, but is even at very large adhesive thicknesses very small. This leads to the conclusion that in the case of a DCB-specimen, only crack propagation in mode I needs to be considered.

6.5 Influence of different shape parameters in model B

In [8] it was claimed that the two shape parameters, V_{1B} and V_{2B} , are of less importance and therefore can be chosen arbitrary. To verify this statement the influence of the shape parameters were investigated. Three different values of parameter combinations have been studied and the behavior of the DCB-specimen can be seen in figure 6.7.

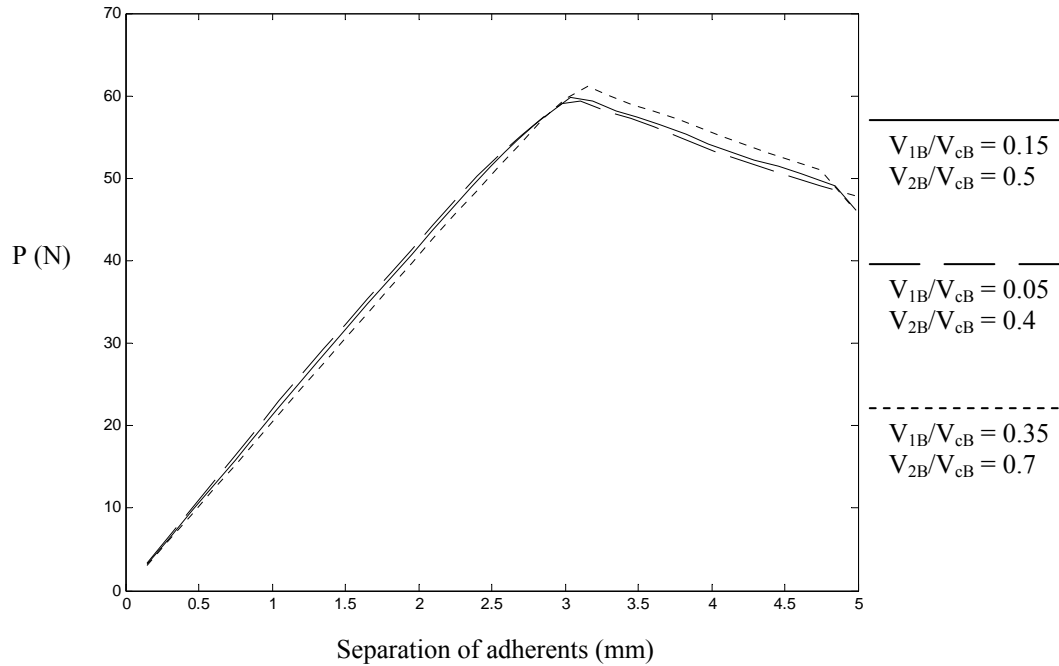


Figure 6.7. Force versus separation of the adherents for different shape parameter combinations.

As seen from figure 6.7 the behaviour of the DCB-specimen is very similar for the different sets of shape parameters. From this the conclusion that the choice of shape parameters are of minor importance when studying the behaviour of a DCB-specimen can be drawn.

6.6 Verification of the finite element model

In order to verify the finite element calculations a simple model of the DCB-specimen, see figure 6.8, has also been studied.

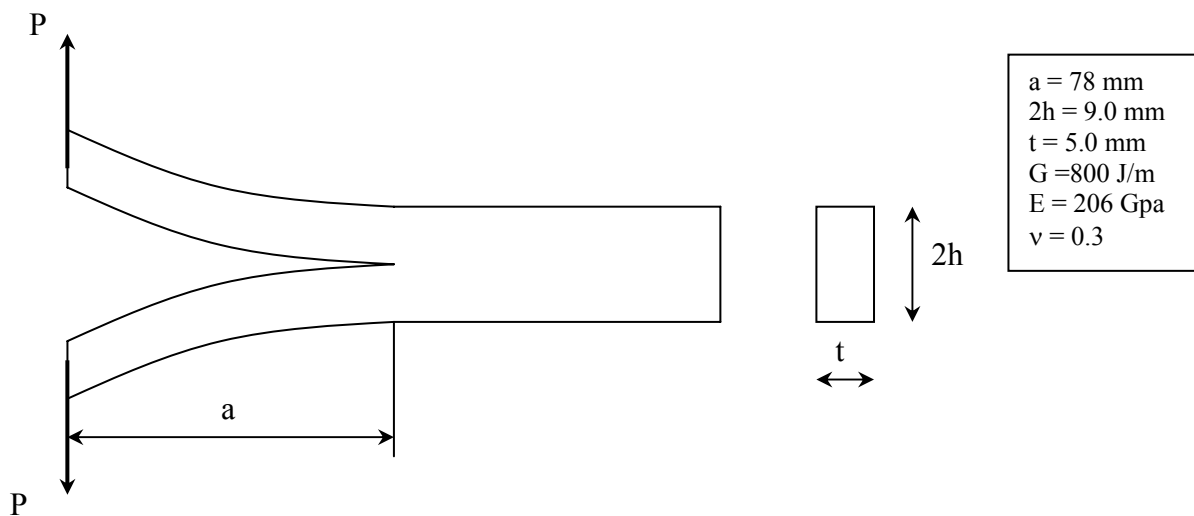


Figure 6.8. DCB-specimen.

From [16] the following equations for the DCB-specimen are obtained:

$$K_I = \frac{2\sqrt{3}P}{th^{1/2}} \frac{a}{hl} \quad (6.1)$$

$$G = \frac{K_I^2}{E'} + \frac{K_{II}^2}{E'} \quad (6.2)$$

where $E' = \begin{cases} E & \text{plane stress} \\ E/(1-\nu^2) & \text{plane strain} \end{cases}$

In the case of a DCB-specimen, only mode I fracture will occur. This conclusion together with equation (6.1) and (6.2) leads to the following equation for calculating the maximum force, P, before fracture occurs:

$$P = \frac{\sqrt{GE'}th^{1/2}}{2\sqrt{3}} \frac{a}{hl} \quad (6.3)$$

Equation (6.3) together with figure 6.8 gives the following results:

$$\left\{ \begin{array}{l} \text{Plane stress: } P_{\max} = 71.7 \text{ N} \\ \text{Plane strain: } P_{\max} = 75.2 \text{ N} \end{array} \right.$$

These results are approximately 10 % higher than the ones obtained by the finite element model for both the plane stress and the plane strain model. This can be explained by the fact that the model of the DCB-specimen used in this chapter is only a rough model of the specimen and therefore not an exact calculation of the maximum force before fracture occurs.

7. Fracture analysis of the lap joint

For the lap joint, two different pre-determined crack paths have been investigated. Along these pre-determined paths cohesive crack elements were placed. The first one is along the centre of the adhesive layer, see figure 7.1.a, and the other at the interface between the adhesive and the upper adherent, see figure 7.1.b. A number of different adhesive thicknesses have also been studied in order to determine how the adhesive thickness influences the global behaviour of the joint.

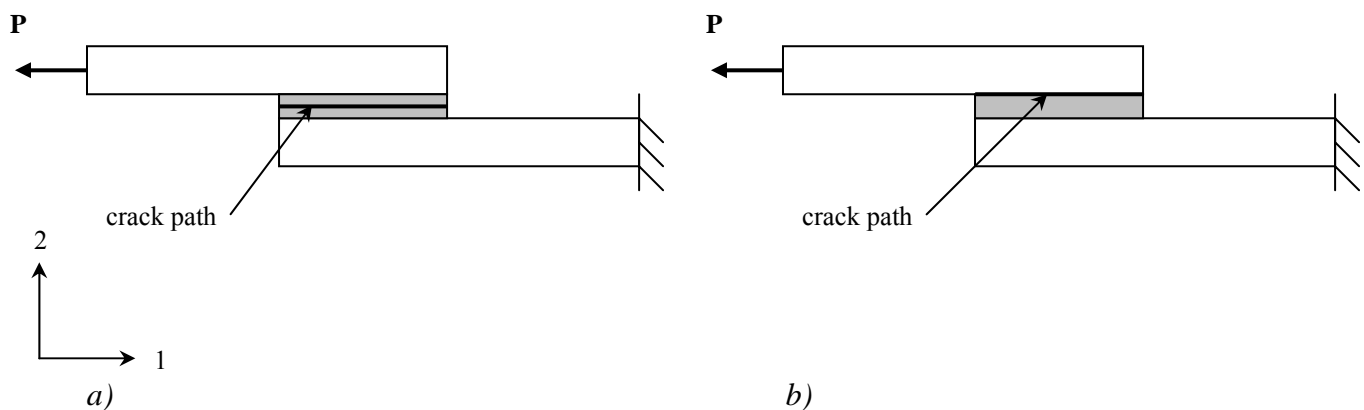


Figure 7.1. Crack paths in the lap joint

7.1 Crack path along the centre of the adhesive layer

In this first part of the analysis of the lap joint the crack elements are placed along the centre of the adhesive layer according to figure 7.1.a. The analysis is displacement controlled, all nodes along the left end of the upper adherent has a prescribed displacement in the 1-direction and the force P is the sum of the reaction forces along this end in the 1-direction. The analysis is performed with three different adhesive thicknesses, 0 mm, 0.1 mm and 0.2 mm for both model A and model B.

During the analysis, some numerical problems were encountered and the analysis diverged. Therefore crack initiation never occurred in the lap joint. Several different step lengths were used but with little success. The behaviour of the lap joint in terms of displacement at the left end of the upper adherent versus the reaction force prior to numerical problems can be seen in figure 7.2.

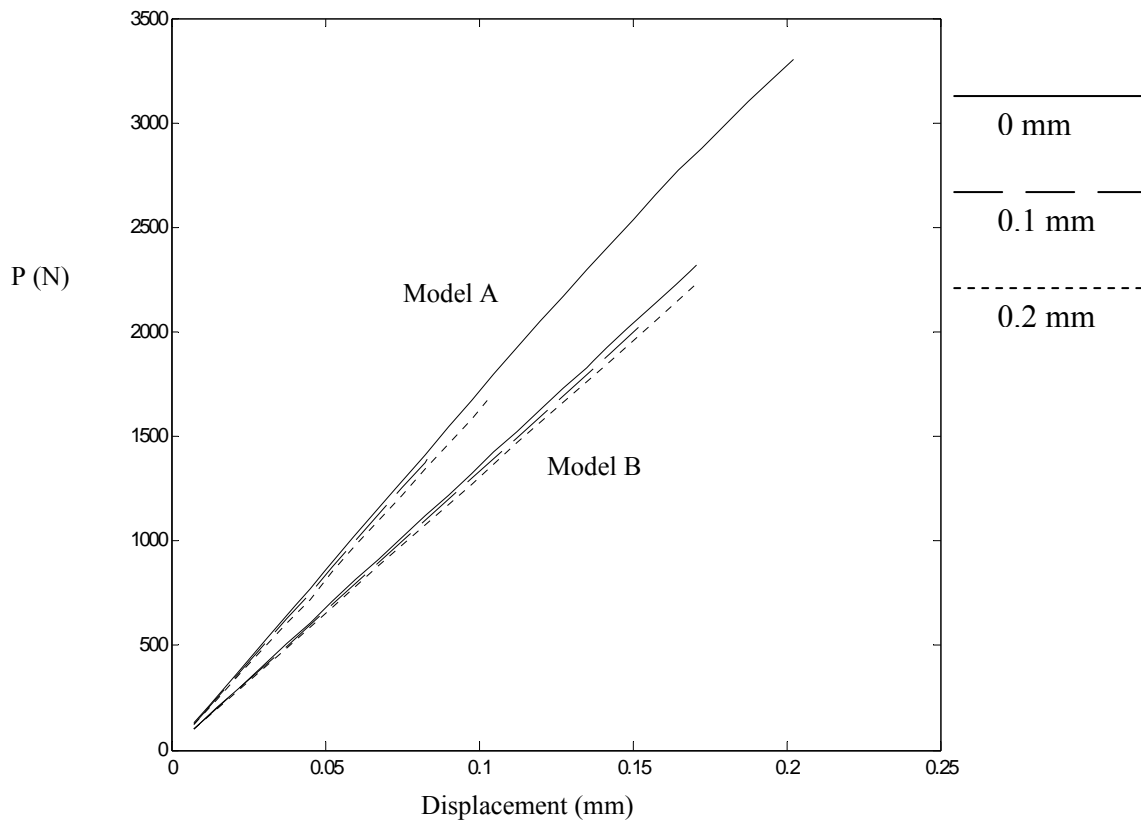


Figure 7.2. Force versus displacement of the end of the upper adherent for both models at different adhesive thicknesses.

As seen from figure 7.2, model B gives a larger displacement at the tip of the adherent for a certain load as compared to model A. This behaviour can be explained by the larger slope of the stress-displacement curves prior to maximum stress level in model A. From figure 7.2 one can also see that the stiffness of the lap joint decreases with increasing adhesive thickness, in both model A and model B.

7.2 Crack path along the interface

An analysis of an interface crack was also performed, see figure 7.1.b, in the same manner as in the case of a crack in the middle of the adhesive. The same numerical problems as described above were encountered. The force versus displacement curves for this case was almost identical to the ones obtained with a crack along the middle of the adhesive shown in figure 7.2.

7.3 Displacements in the adhesive

In order to fully understand the behaviour of the lap joint an analysis of the displacement in both the 1- and 2-direction along the crack path was performed. The displacements, V_1 and V_2 , in the case of a crack path along the centre of the adhesive are defined according to figure 7.3.

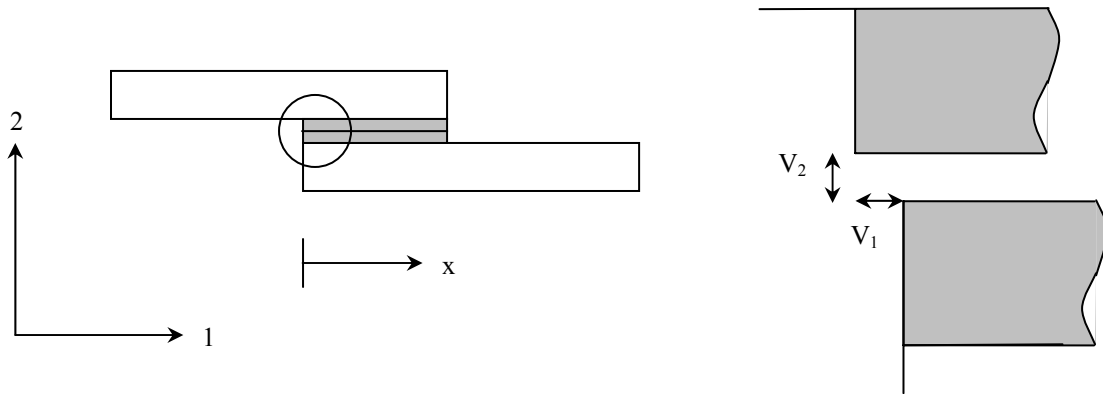


Figure 7.3. Description of the test configuration.

An adhesive thickness of 0.2 mm was used and the analysis was performed with a prescribed displacement of 0.103 mm at the end of the upper adherent. This is the largest displacement before numerical problems occur for model A. In order to compare the two different models the same displacement is also used for model B. The analysis is performed for both the different crack paths. The results from a crack path along the centre of the adhesive layer are seen in figure 7.4 and 7.5. The definition of the displacements, V_1 and V_2 , in the case of an interface crack was made similar to that for a crack in the centre of the adhesive, see figure 7.3.

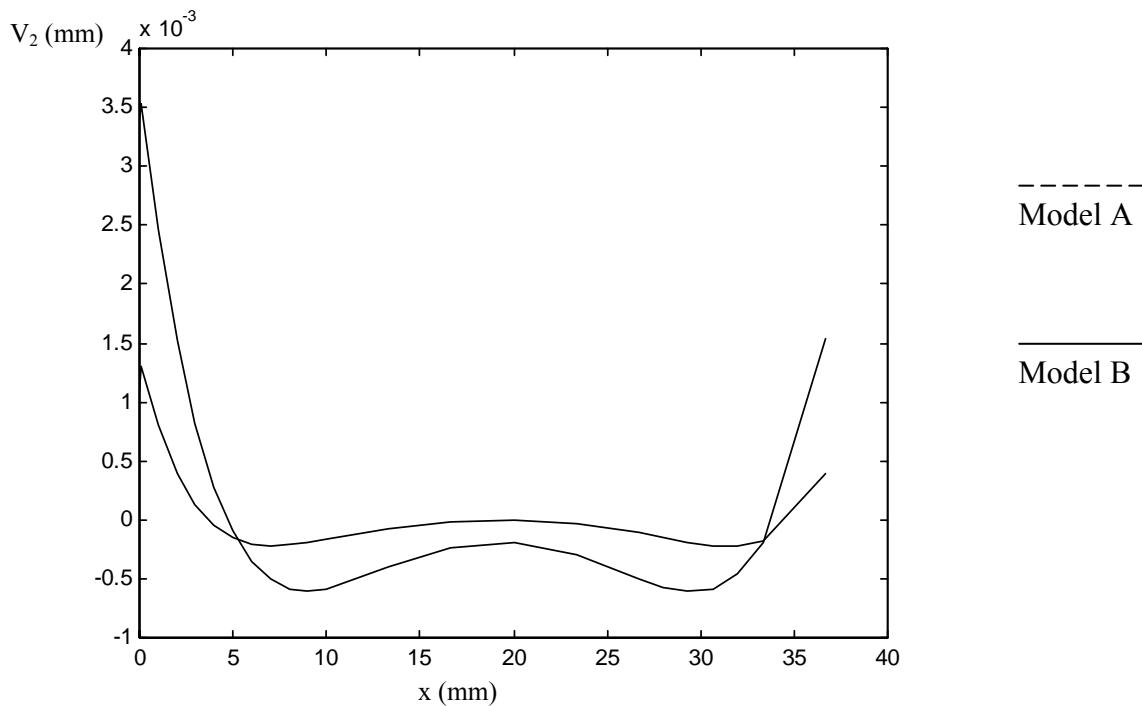


Figure 7.4. Adhesive displacement in the 2-direction.

From figure 7.4 it is seen that the largest displacements in the 2-direction occur at the ends of the adhesive layer. With increasing x , the displacement decreases to a point where it changes to be a compression of the adhesive. The displacement in the 2-direction in the adhesive is almost symmetric around half the adhesive length. The absence of calculated values for $x > 37$ mm is explained from that due to numerical problems, no crack elements could be placed at the right end of the adhesive layer. From figure 7.4 it is also seen that model A gives smaller displacements in the adhesive as compared to model B since model A is stiffer than model B.

The same analysis was also performed with a crack path along the interface between the upper adherent and the adhesive. The results were almost identical with the ones obtained with a crack path in the centre of the adhesive layer. The only difference between the two crack paths was that the displacements at the ends of the adhesive were somewhat larger for an interface crack path. This can be explained by the high stiffness of the adherents in comparison to the adhesive layer.

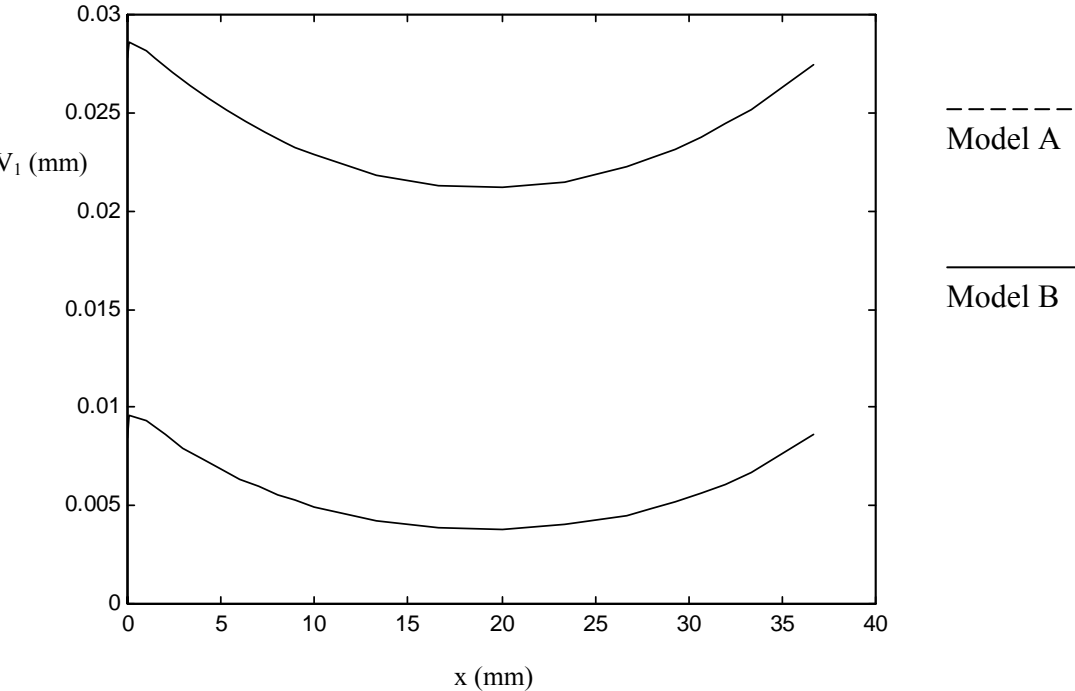


Figure 7.5. Adhesive displacement in the 1-direction.

Figure 7.5 shows the displacement in the 1-direction, corresponding to figure 7.4. It is seen that the largest displacements in the 1-direction occur at the ends of the adhesive layer. With x increasing from zero, the displacement decreases to a point where it reaches a minimum value as x equals, approximately, half the adhesive length. The displacement in the 1-direction in the adhesive is almost symmetric around half the adhesive length. It is also seen that the displacement in the 1-direction does not vary so much with x as in the 2-direction. From figure 7.5 it is also seen that model A has smaller displacements in the adhesive as compared to model B. This is because model A is stiffer than model B.

A similar analysis was also performed with a crack path along the interface between the upper adherent and the adhesive. The only difference in results between the two different crack paths was that the displacements in the 1-direction at the ends of the adhesive were larger with an interface crack path. The difference was however very small. This result can be explained by the high stiffness of the adherents in comparison to the adhesive layer.

8. Summary and discussion

From the finite element calculations with the model without cracks, the most critical location as regards crack propagation in the adhesive could be estimated. The critical location was at the interface between the adhesive and adherent for both the DCB-specimen and the lap joint. This location was chosen as one prescribed crack path. Another one was chosen along the center of the adhesive layer.

Along the presumed crack paths, special finite elements with different stress-separation laws were included. The first, model A, had proportional stress-displacement relations at loading and unloading. The second one, model B, included a plateau at maximum stress level.

From the analysis of the DCB-specimen the conclusion that the adhesive thickness does not influence the behavior of the joint was drawn. The critical load when the crack starts to grow was determined for two different models. The results also showed that model B starts to crack at a lower load than model A. When comparing the two different crack paths it was concluded that no difference in the global behavior of the joint could be seen. Therefore, no assumption of which crack path that is more likely than the other could be drawn after crack propagation actually was initiated. The stress analysis prior to crack growth indicated, however, that the most probable site for crack initiation is in the adherent/adhesive interface. The crack length as a function of horizontal displacement was also studied. From this study, it was concluded that an approximately linear relation between the horizontal displacement of the adherent and the crack length exists, see figure 6.6.

The analysis of the lap joint could not be concluded due to numerical problems, therefore no critical load could be determined for this case. However, from the results of the analysis prior numerical problems it was seen that an increase of adhesive thickness causes an increase of vertical displacement in the adherent at a given load. The vertical and horizontal displacements along the adhesive were also studied. The largest displacements were found at the ends of the adhesive layer. Also, the displacements were approximately symmetric around half the adhesive length. From the analysis of the different crack paths only small differences were encountered. The largest discrepancy occurred at the ends of the adhesive layer where the interface crack path results in higher displacements in both directions. From these results one can conclude that the lap joint probably will crack at the interface between the adherent and the adhesive. However, the difference is very small.

Since no difference between the behavior with respect to critical displacement of the DCB-specimen with the two crack paths could be detected no conclusions about the preferred crack path can be drawn. In order to do this, another approach to the problem is obviously needed, such as determining the stress intensity factors at different locations of an existing small crack.

The numerical problems that occurred in the analysis of the lap joint might be explained from figure 7.5. In the figure, it is seen that all the elements in the adhesive layer have approximately the same horizontal displacement and this may cause numerical problems. The same problem with determining the preferred crack path in the lap joint as in the DCB analysis also exists. However, a small difference at the ends of the adhesive layer can be seen in the lap joint for different crack paths, but the difference is very small.

Future work would be to develop a new crack element that works together with the lap joint geometry. It might well be that fracture occurs at a position where an imperfection of some kind is situated. The advantage with the method used in this paper is the possibility to follow the crack growth in the joint as the vertical displacement of the adherent is increased.

9. Conclusion

Crack initiation and growth in mixed mode in adhesive joints can be modeled introducing special crack elements with prescribed piece wise linear stress-separation relations that gradually relaxes the binding stresses along the crack path until total relaxation of the element is achieved. It was found that the characteristic parameters of such a stress-separation law where the maximum stress and largest separation that can be accommodated by the crack element.

It was found that the thickness of the adhesive as regards crack propagation is of minor importance. Also the choice of plane stress or plane strain was shown to be of less importance.

11. References

- [1] H. Chen, L. Wang, B.L. Harihaloo and F.W. Williams, Fracture analysis for multi-material system with an interface crack, *Computational Materials Science* 12 (1998), pp. 1-8.
- [2] O. Avila-Pozos, A. Klarbring and A.B. Movchan, Asymptotic model of orthotropic highly inhomogeneous layered structure, *Mechanics of Materials* 31 (1999), pp. 101-115.
- [3] N.S. Ottosen and K.G. Olsson, Hardening/Softening Plastic Analysis of Adhesive Joint, *Journal of Engineering Mechanics* Vol. 114 No 1 (1988), pp. 97-116.
- [4] R.H. Andruet, D.A. Dillard and S.M. Holzer, Two and three-dimensional geometrical nonlinear finite elements for analysis of adhesive joints, *International Journal of Adhesion & Adhesives* 21 (2001), pp. 17-34.
- [5] H. Ljungquist, Constitutive Modelling of Adhesive Joints and Application to Impact Analysis for a Truck Cab Using the Finite Element Method, Division of Solid Mechanics, Chalmers University of Technology (1997).
- [6] V. Tvergaard and J.W. Hutchinson, On the toughness of ductile adhesive joints, *J. Mech. Phys. Solids* Vol. 44 No5 (1996), pp. 789-800.
- [7] Q.D. Yang and M.D. Thouless, Mixed-mode fracture analyses of plastically-deforming adhesive joints, *International Journal of Fracture* 110 (2001), pp 175-187.
- [8] Q.D. Yang, M.D. Thouless and S.M. Ward, Elastic-plastic mode-II fracture of adhesive joints, *International Journal of Solids and Structures* 38 (2001), pp 3251-3262.
- [9] J. Guillemenet and S. Bistac, Crack propagation in adhesively bonded steel assemblies, *International Journal of Adhesion & Adhesives* 21 (2001), pp. 77-83.
- [10] T. Andersson and U. Stigh, Verifacation of an experimental method to measure the stress-elongation law for an adhesive layer using a DCB-specimen, Department of Engineering Science, University of Skövde.
- [11] T. Andersson and U. Stigh, An experimental method to determine the complete stress-elongation relation for a structural adhesive layer loaded in peel, Department of Engineering Science, University of Skövde.
- [12] T.L. Anderson, *Fracture Mechanics Fundamentals and applications*, Second Edition, CRC Press (1995), pp. 75-77.

- [13] Hibbit, Karlsson and Sorensen INC, "ABAQUS/standard User's Manual , Vol. I-III", Pawatucket, USA, Version 5.8 (1998).
- [14] M. Andersson, Formulering och implentation av interfacelement för abaqus, Department of Mechanical Engineering, Lund Institute of Technology (2000).
- [15] N. Ottosen and H. Petersson, Introduction to the Finite Element Method, Prentice Hall Europe (1992), pp. 292-310.
- [16] B. Sundström, Handbok och formelsamling i Hållfasthetslära, Institutionen för Hållfasthetslära KTH (1998), pp. 235-276